Project Final Report

August 31, 2021

DOE Cooperative Agreement

DE-FE0031718

DOE-UCLA-FE0031718

A Scalable Process for Upcycling Carbon Dioxide (CO_2) and Coal Combustion Residues into Construction Products

Submitted by

University of California, Los Angeles (UCLA)

420 Westwood Plaza

Los Angeles, CA, 90095

Principal Investigator

Gaurav N. Sant

310-206-3084

gsant@ucla.edu

Submitted to

U.S. Department of Energy

Office of Fossil Energy

National Energy Technology Laboratory

Disclaimer

0 Table of Contents

1 Introduction

1.1 Background

Anthropogenic sources of carbon dioxide are generated from a number of sources, but the key among these are ordinary Portland cement (OPC) production and combustion of fossil fuels [1]. Cement production is the largest global CO_2 source from the mineral decomposition of carbonates [1]. This is due to the clinkering process whereby limestone (mainly consisting of $CaCO_3$) is decomposed into CaO and CO_2, and combined with silica rich clays at high temperatures to form clinkers (i.e. the four key minerals that comprise cement) [2]. The high temperature range of 1400 – 1550 °C required for this process accounts for up to 60% of the generated CO_2 from cement production [3]. Combination of the limestone decomposition and thermal requirements of the clinkering process causes cement production to contribute 8-9% of annual global CO_2 emissions [1,2,4–6]. Combustion of fossil fuels (coal, oil and gas) was shown to contribute a much larger portion of global CO_2 emissions. As of 2018, combustion of fossil fuels accounted for 65% of global CO_2, where 41% was derived from stationary sources for electricity and heat generation and the other 24% was related to transport [7]. To reduce these contributions, key steps forward in CO_2 utilization technologies are required. Therefore, a CO_2 mineralization technology (CO_2 mineralization concrete) to reduce the OPC content in concrete, while utilizing flue gas emissions from fossil fuel combustion has been developed to address both areas simultaneously.

This Reversa™ technology utilizes low-carbon cementation agents produced by *in situ* CO_2 mineralization ("mineral carbonation reactions") to offer a promising alternative to OPC [8–12]. CO_2 mineralization relies upon the reaction of dissolved CO_2 with inorganic alkaline reactants to precipitate mineral carbonates (e.g., $CaCO_3$), which bind proximate particles and achieve cementation [9,12–14]. Herein, a concrete *green body*, that is composed of a mixture of binder, water, and mineral aggregates, is exposed to CO_2 borne in industrial flue gas streams. This manner of CO_2 mineralization allows the production of construction components that feature equivalent engineering attributes as their OPC-based counterparts while featuring a much smaller embodied carbon intensity (eCI).

The purpose of this project is to demonstrate the feasibility of the Reversa process evolving from a TRL-3 technology at the bench-scale up to TRL-6 technology at the pilot-scale. The reliability of the Reversa technology was tested to prove the effective production of concrete masonry units (CMUs) at bench scale, where the units exceeded the required 13.8 MPa compressive strength requirements [14,15]. The results detailed herein will demonstrate the evolution of this technology to the industrial scale. The culmination of this work resulted in 6 production runs were completed at the National Carbon Capture Center (NCCC), Wilsonville, AL, using coal-fired and natural gas (NG) flue gas as the CO_2 source. This was the second site demonstration performed using this technology following 12 successful production runs at the Integrated Test Center (ITC), Gillette, WY. Over the course of the production runs at NCCC and ITC, the CO_2 utilization as a function of time, 24-h CO_2 uptake, electricity usage, and 28-d net area compressive strength recorded for each run. Collection of this data will be used to determine the success of the demonstration goals: (1) achieving in excess of 75% CO_2 utilization efficiency, (2) utilizing greater than 250 kg of CO_2 per production batch/run, and (3) ensuring compliance of carbonated blocks with industry standard specifications (ASTM C90 [15]).

1.2 Objectives

The overall goal of this project is to accelerate the development of a CO_2 mineralization process that synergistically utilizes CO_2 in flue gas and coal combustion residues (CCRs) to synthesize carbonated concrete, a functional replacement for traditional concrete. Over the course of this project, the Recipient will design, fabricate, and optimize a field-scale CO_2 processing (carbonation) system designed to consume about 100 kg of CO_2 per day directly from coal-derived flue gas, without a CO_2 capture or enrichment step. The Recipient will evaluate the system's performance at two suitable host sites using real coal flue gases, during which critical data on energy inputs and CO_2 uptake rates achievable at the field-scale will be compiled. The performance data and optimization sequence that the Recipient collects will inform design and scaling analysis required for development of a commercial-scale CO_2 mineralization system, which will be achieved prior to the completion of this project.

1.3 Scope

The Recipient will finalize the Project Management Plan including inputs provided by DOE. The Recipient will characterize the carbonation kinetics of CCRs and hydrated lime to establish bounds for selection/acceptance criteria for use in carbonated concrete formulations. The Recipient will evaluate the effects of processing conditions, such as temperature (T), relative humidity (RH), and CO_2 partial pressure (p_{CO2}), on heat and mass transfer of carbonated concrete as a function of gas flow rate. The Recipient will deliver a detailed design of a *beta* prototype Reversa processing system. The completed system will be fabricated, commissioned, and performance optimized. The optimized *beta* Reversa carbonation system will be field-tested at two suitable host sites using coal-derived flue gas. A detailed techno-economic analysis (TEA) and lifecycle analysis (LCA) will be carried out to support development of a commercial-scale carbonated concrete production facility.

2 Task 1.0 – Project Management and Planning

2.1 Project Organization

Prof. G. Sant was responsible for the overall project management and coordination, with assistance from research management staff at UCLA. Prof. Sant directed the team at UCLA and ensured close collaboration between the academic and industrial partners in ensuring that tasks are accomplished on-time and on budget. He was responsible for day-to-day management of the project and coordination between different faculty, external collaborators, and DOE. He was responsible for scheduling meetings, teleconferences and in-person meetings as needed. Project progress was tracked using templates and project management software (MS Project 2013), with inputs provided by the faculty responsible for individual tasks. Emphasis was placed on tracking task timelines, and project milestones/deliverables to assess success levels related to specific tasks. Dr. Sant was also responsible for developing reporting and/or scientific documents based on the project. He oversaw all aspects related to the scientific direction, with support from the research management staff at UCLA towards financial management. Each collaborator assumed primary responsibility for the completion of the tasks led by them (see organization and task leads in Table 1), reporting to the wider team, and preparing reports and scientific documents related to their tasks. Dr. Sant also convened meetings with the funding agency, reported project progress and took remedial actions to ensure on-time completion.

Multi-institutional activities require project progress and critical paths to be managed efficiently to ensure success. The PIs worked closely with each other and partners (e.g. Susteon and Air Clean Systems) to ensure that there were minimal impediments to the critical paths. In case of a path-block or conflict, the PI was in close communication with the partners and Co-PIs to seek resolution. Careful strategies in risk management were designed to: (i) understand if the risk may prevent or delay the research outcomes, (ii) understand the causal factors of risk and the threat of its propagation, and (iii) develop contingency plans and identify less-risky solutions.

Scientific publications and presentations which are outcomes of multiple institution/investigator efforts were circulated to the team for inputs before presentation/submission for publication. If conflicts arise, they were mediated by the PI after seeking inputs, and collecting facts from all stakeholders. A comprehensive agreement on intellectual property (IP) developed during the project is a cornerstone of a successful market-oriented exploitation. Thus, the technology transfer offices at partner institutions ensured that any IP arising out of the project is protected. It is agreed that the IP is owned by the institution that develops it. In the event of multiple partners being involved in IP development, licensing agreements were executed between the partners through IIAs. The IP teams carried out market analysis, competitor summary and risk assessments, and developed IP protection plans. A flexible and efficient mechanism to support cooperation between partners, to guarantee protection and maximum use of results as well as to ensure immediate dissemination of the research results was implemented.

Table 1: Project organization chart indicating primary personnel responsible for each task and subtask. Lead personnel for each task are denoted in bold type, with support personnel in normal typeface.

Task	Description	Lead	Support Personnel			
1	Project Management and Planning	**G. Sant**	Project Scientist 1	Project Scientist 2	R. Kaner	
2	Material specifications, acceptance criteria, and component performance	**G. Sant**				
2.1	Sourcing and characterization of CCRs and portlandite	**Project Scientist 1**	Project Scientist 2	G. Sant	R. Kaner	GSR
2.2	Carbonation kinetics of reactants	**Project Scientist 2**	Project Scientist 1	G. Sant	R. Kaner	GSR
2.3	Component performance	**Project Scientist 1**	Project Scientist 2	G. Sant	R. Kaner	GSR
3	Bench-scale studies to acquire critical data for system design	**G. Sant**				
3.1	Process conditions of simulated flue gas	**Project Scientist 2**	Project Scientist 1	G. Sant	R. Kaner	GSR
3.2	Quantification of heat and mass transfer in CO_2NCRETE process	**Project Scientist 1**	Project Scientist 2	Process Eng.	B. Turk	R. Gupta
4	Design and fabrication of modular, scaled CO_2 processing system	**Process Eng.**				
4.1	Component selection and system design	**Process Eng.**	B. Turk	R. Gupta	Project Scientist 1	Project Scientist 2
4.2	System construction	**Project Scientist 1**	Project Scientist 2	G. Sant	R. Kaner	GSR

5	Commissioning and trial operation of the CO_2NCRETE production system	**Project Scientist 2**				
5.1	System start-up/commissioning	**Project Scientist 1**	Project Scientist 2	Process Eng.	B. Turk	G. Sant
5.2	System performance validation	**Project Scientist 2**	G. Sant	R. Gupta	R. Kaner	GSR
6	Field demonstration of CO_2NCRETE carbonation system	**G. Sant**				
6.1	Host site preparation	**Project Scientist 1**	Project Scientist 2	G. Sant	R. Kaner	GSR
6.2	Test plan development	**Project Scientist 1**	Project Scientist 2	G. Sant	R. Kaner	GSR
6.3	Installation and operation	**Project Scientist 2**	Project Scientist 1	Process Eng.	B. Turk	R. Gupta
6.4	Decommissioning	**Project Scientist 2**	Project Scientist 1	G. Sant	R. Kaner	GSR
7	Design and scalability analysis for commercial-scale CO_2NCRETE system	**Process Eng.**	B. Turk	R. Gupta	G. Sant	Project Scientist 2
8	Techno-economic analysis (TEA) and life cycle assessment (LCA)	**G. Sant**				
8.1	Technology maturation plan	**Project Scientist 1**	Project Scientist 2	G. Sant	R. Kaner	GSR
8.2	Techno-economic analysis	**Process Eng.**	B. Turk	R. Gupta	Project Scientist 1	Project Scientist 2
8.3	Life cycle analysis	**R. Kaner**	GSR	Project Scientist 1	Project Scientist 2	G. Sant

8.4	Technology gap analysis	**Project Scientist 2**	Project Scientist 1	G. Sant	R. Kaner	GSR

2.2 Risk management plan

Figure 1: The risk management approach that will be followed in this project.

This project had specific types of risks due to its size, scope, nature and maturity of the technology as well as managerial approach, which have been summarized in Table 2. The PI and a project manager will closely monitor the scientific/financial aspects of the project to ensure that risks are identified early and promptly resolved using Table 2 as the initial risk registry (see Figure 1 for risk management approach). The probability of occurrence of a risk and its impact on the project are also recorded in Table 2. The probabilities and impact classifications were based on the original understanding of the readiness of the technology and the team's competencies.

Over the course of the project, the project team monitored the elements of risk noted in the risk registry and added new risks as they were identified. Each team member was assigned to monitor the risks that are related to their tasks. As the probability of occurrence for any risk increases, the team member responsible for the risk should establish suitable mitigation strategies and begin prompt implementation of these strategies when predefined criteria are met. The risk register will help the PI and team members track, monitor, and decide when mitigation strategies need to be implemented. The risk register was accessible to all team members and regularly updated by the PI based on regular risk management team meetings held throughout the project.

Table 2: An initial risk-register identifying anticipated project risks, their probability and iMPact, and mitigation/response strategies.			
Description of Risk	**Probability (Low, Moderate, High)**	**Impact (Low, Moderate, High)**	**Risk Management Mitigation and Response Strategies**
Financial Risks:			
Budget shortfalls	Moderate	High	Closely monitor project costs and scope and set spending priorities based on timelines and milestones. Conduct periodic (weekly) meetings with team and utilize detailed task tracking application.
Cost/Schedule Risks:			
Cost of system fabrication exceeds initial estimates	Low	Moderate	Perform detailed design and collect estimates from vendors and fabricators from early project stages
Duration of system fabrication exceeds initial estimates	Low	Moderate	Closely manage project progress and system development with the fabricator and system integration team through periodic (weekly) meeting and detailed tracking of team deliverables.
Delayed delivery of supply	Moderate	Low	Anticipate supplies, pre-order, and track key/critical components to ensure that their delivery is on time or schedule changes are implemented to accommodate the delay reduce/eliminate delays through risk-based management of supplies
Technical/Scope Risks:			
Coal combustion residues shows slow carbonation	Moderate	Low	Adjust the proportions of $Ca(OH)_2$/fly ash, and/or secure calcium-rich fly ash (i.e., higher CaO content)

kinetics and/or low carbonation potential			
Concrete slurry shows unsatisfactory workability	Moderate	Low	Adjust workability with rheology modifiers (e.g., viscosity modifiers, and dispersants)
Carbonated concrete shows unsatisfactory strength	Low	Low	Enhance strength by pre-carbonation densification to reduce porosity reduction, and/or add inorganic binders to the formulation
Scope creep	Moderate	Moderate	Set and closely monitor clear priorities and assign resources based on timelines and milestones defined in formal project management plan. Maintain clear communications between teams through periodic meetings and standardized communications such as weekly project updates.
Planning and Oversight Risks:			
Inexperienced staff	Low	Low	Schedule sufficient time for training of new staff and technicians utilizing standardized training modules
EH&S Risks:			
Environmental permitting	Moderate	High	Begin permitting discussions early in the project's lifecycle to fully understand permitting requirement and timing
Control of flue gas exhaust and fugitive dust	Moderate	Moderate	Provide proper engineering controls to mitigate exposure to dust/flue gas in full compliance with State and Federal requirements
Materials handling related safety issues	Low	Moderate	Follow all relevant CALOSHA/OSHA regulations for workplace safety; develop written procedures with UCLA's EH&S staff and conduct

			periodic assessments to assure compliance
External Factor Risks:			
Inability to source relevant CCRs	Low	Low	Reduce scope of CCRs, source fly ashes directly from utility sites
Closure/lack of access to demonstration site	Low	Low	Collaborate with facility staff to alter scheduling and/or secure access to an alternate demonstration facility
Host Site Risks:			
Loss of flue gas at the host site	Low	High	Maintain close communication with host site staff regarding planned outages; secure simulant flue gas as back-up measure for operational trials
Loss of utilities at the host site	Low	High	Maintain close communication with host site staff regarding planned outages; secure back-up generator and process water for operational trials
Integration issues (e.g., connection of system to host site, control of flue gas into system)	Moderate	High	Get sign-off on integration strategy from host site operators in design reviews; develop and discuss operational plan
Insufficient product storage and/or delayed product transportation	Moderate	Moderate	Develop strategy for on-site product storage including transportation schedule; identify secondary off-site storage in proximity of host site
Management Risks:			
Delayed finish of earlier projects	Moderate	Moderate	Closely and formally track project progress and develop alternative pathways when delays emerge. Ensure timely delivery of independent research activities when delays emerge.

Losing critical staff at crucial point of the project	Low	Moderate	Training multi-skilled, cross-trained staff and establish clear written standard operating procedures for interoperability and flexibility

3 Task 2.0 – Material specifications, acceptance criteria, and component performance

3.1 Sourcing and characterization of CCRs and portlandite (CH)

Twenty-three coal combustion residues (CCRs) were procured in varying quantities (i.e., ranging from ≈ 250 g to 150 kg each). The chemical (oxide) composition of each CCR was determined using X-ray fluorescence (XRF) following ASTM D4326,[16] as shown in Table 2. The CCRs include 21 fly ashes (FA) and 2 bottom ashes (BA). The CCRs span a wide range of chemical compositions, reflecting diverse coal sources and emissions control steps. The procured CCRs were selected to feature aspects that make them undesirable for use in conventional concrete.

Many of the procured CCRs feature elevated sulfur trioxide (SO_3) contents, in excess of the 5.0 mass % limit specified in ASTM C618,[17] rendering them unsuitable for use in conventional concrete mixture formulations. Other CCRs feature excessive carbon contents (i.e., loss on ignition), suffer from poor fineness, or feature elevated chlorine contents. Chlorine (Cl) was not specifically accounted for in the standard XRF analysis, but those CCRs with low "Total" compositions (i.e., < 98 mass %) were expected to feature elevated chlorine contents. Indeed, and additional analysis revealed that CCRs # 9, 10, and 19 featured 12.6 mass %, 1.76 mass %, and 6.83 mass % Cl, respectively. The remainder of difference between the total mass composition and 100 % can be attributed to trace oxides. The oxide composition of a CCR determines its theoretical carbonation potential (i.e., the maximum mass of CO_2 that may be taken up per mass of reactant) as described by the Steinour equation:[18] $m_{CO_2}^{max} = 0.785\left(m_{CaO} - 0.560m_{CaCO_3} - 0.700m_{SO_3}\right) + 1.091m_{MgO} + 0.71m_{Na_2O} + 0.468m_{K_2O}$, where m_i represents the mass percent of oxide "*i*" present in the CCR. As CCRs feature little magnesium, sodium, and potassium oxides, (i.e., < 10 mass %), their theoretical carbonation potentials are dominantly controlled by their calcium oxide (CaO) content. Therefore, this descriptor is generally in-line with the standardized classifications of fly ashes, whereby Class C ashes (m_{CaO} > 18.0 %, i.e., calcium-rich) demonstrate greater carbonation potentials than Class F ashes (m_{CaO} ≤ 18.0. %, i.e., calcium-poor). The presence of SO_3 in certain calcium-rich CCRs is of interest as it reduces their carbonation potentials. This is apparent in CCRs such as CCR # 1, 2, 3, 4, 9, 10, 17, 19, and 23, which likely contain gypsum ($CaSO_4{\cdot}2H_2O$) resulting from flue gas desulfurization.

Seven grades of portlandite (i.e., hydrated lime, $Ca(OH)_2$) were procured. The purity of hydrated lime reactant was given by the manufacturers, and ranged from 61.1 mass % to 94.0 mass % $Ca(OH)_2$. The theoretical carbonation potential of the portlandite reactants may be assessed simply via the stoichiometry of the carbonation reaction $Ca(OH)_2 + CO_2 \rightarrow CaCO_3 + H_2O$, which provides a theoretical maximum of 0.59 g CO_2 / g $Ca(OH)_2$. The impurities in the portlandite reactants comprise MgO or $Mg(OH)_2$ and trace amounts of CaO, which may carbonate, but with greatly retarded kinetics relative to $Ca(OH)_2$ within relevant process conditions, as well as $CaCO_3$ (i.e., pre-carbonated reactant). These phases typically demonstrated negligible contributions to the CO_2 uptake of portlandite reactants, under the process conditions utilized herein.

Table 3. Chemical composition of the 23 types of coal combustion residues (CCRs) procured, determined by X-ray fluorescence (XRF) as mass % of oxide.

CCR #	Composition (mass %)												
	SiO_2	Al_2O	Fe_2O_3	SO_3	CaO	Na_2O	MgO	K_2O	P_2O_5	TiO_2	SrO	BaO	Total
1	35.49	17.26	5.00	7.85	26.32	0.93	3.17	0.45	0.66	1.19	0.22	0.40	98.94
2	33.34	16.34	4.79	9.27	26.43	1.24	4.52	0.56	0.83	1.23	0.26	0.51	99.32
3	29.43	16.71	5.14	12.29	25.78	2.34	3.65	0.48	0.84	1.23	0.26	0.44	98.58
4	26.09	14.51	3.88	11.95	33.72	1.20	3.65	0.34	0.84	1.16	0.28	0.46	98.08
5	54.46	23.14	11.72	0.48	2.79	1.52	1.18	2.37	0.36	1.17	0.12	0.24	99.56
6	66.31	15.54	9.91	1.19	1.85	1.41	0.92	1.09	0.12	0.69	0.09	0.21	99.32
7	52.02	22.49	14.70	0.34	2.73	0.87	0.91	2.55	0.21	1.20	0.07	0.09	98.19
8	27.81	19.08	5.80	2.44	30.12	1.82	7.20	0.35	1.78	1.45	0.47	0.92	99.24
9	9.76	4.86	2.71	18.71	47.61	0.11	2.33	0.12	0.12	0.22	0.02	0.01	86.57
10	36.08	16.86	11.69	6.39	20.75	0.79	1.37	1.78	0.21	0.92	0.07	0.05	96.95
11	43.85	17.64	6.76	1.42	21.39	1.09	4.40	0.46	0.63	1.40	0.27	0.48	99.80
12	52.02	24.44	12.01	1.11	3.41	0.86	0.91	2.52	0.16	1.34	0.07	0.12	98.98
13	51.21	27.48	5.91	2.68	5.22	0.26	1.00	2.51	0.15	1.44	0.07	0.12	98.05
14	42.03	18.92	3.53	2.81	27.47	0.43	1.04	1.37	0.34	0.92	0.10	0.12	99.08
15	43.95	20.40	22.48	1.35	5.45	2.02	0.82	1.92	0.25	1.03	0.09	0.06	99.80
16	45.55	23.10	20.54	0.51	1.39	3.08	0.67	2.14	0.41	1.27	0.10	0.06	98.80
17	39.25	19.82	4.47	7.97	14.38	5.91	3.61	1.04	0.94	1.37	0.22	0.49	99.46
18	53.92	21.21	16.23	0.44	3.28	0.49	0.79	2.03	0.17	1.15	0.06	0.13	99.89
19	16.40	7.59	4.41	13.45	46.78	0.41	1.86	0.71	0.12	0.42	0.04	0.03	92.23
20	54.48	29.94	7.04	0.11	1.19	0.37	1.02	2.91	0.58	1.55	0.13	0.13	99.44
21	47.68	23.62	19.47	0.52	2.59	0.48	1.75	1.99	0.29	1.20	0.11	0.08	99.78
22	48.53	23.99	16.81	1.99	1.79	2.06	0.67	2.09	0.13	1.31	0.08	0.09	99.57
23	22.77	11.99	3.97	12.58	38.48	1.98	4.91	0.22	0.73	0.86	0.35	0.47	99.29

The CO_2 uptake of each CCR and portlandite reactant was assessed experimentally using custom-built bench-scale carbonation reactors (Figure 2). The reactors consist of cylinders with an internal diameter of 100 mm and a length of 150 mm, which were placed in an oven for temperature regulation. The inlet gas was composed by mixing air and CO_2 using mass flow controllers to mimic the exhaust of a coal power

plant [19]. The gas is composed of 12 ± 0.2 % CO_2 [v/v] as confirmed using gas chromatography (GC; F0818, Inficon). The gas mixture was flowed through gas washing bottles placed in a separate oven with independent temperature control, to alter the saturated vapor pressure and evaporation rate of water, as a means to control the relative humidity (RH) of the gas stream. Three replicate samples of approximately 0.5 g of each reactant were placed within sample cells in each reactor. After 30 minutes of equilibration to the RH and temperature of an inert gas stream, CO_2 exposure was initiated for a total duration of 24 h. Reactor conditions were maintained to T = 65 °C, RH ≈ 80 %, and [CO_2] ≈ 12 %.

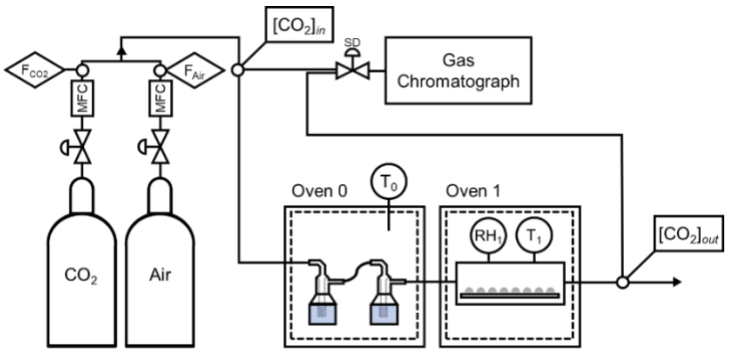

Figure 2: A schematic of the bench-scale carbonation reactor system used for CO_2 uptake experiments, including gas mixing, flow rate control, and monitoring and control of relative humidity (RH) and temperature (T) within the reactors.

The CO_2 uptake after 24 h of CO_2 exposure was quantified using thermogravimetric analysis (TGA: STA 6000, Perkin Elmer). Around 30 mg of each powder was placed in pure aluminum oxide crucibles and heated at a rate of 15 °C/min over a temperature range of 35 °C to 975 °C under UHP-N_2 gas purge at a flow rate of 20 mL/min. The CO_2 uptake was quantified by assessing the mass loss associated with $CaCO_3$ decomposition over the temperature range of 550 °C to 900 °C,[13] normalized by the mass of reactant solids (i.e., excluding evaporable water).

Figure 3(a) displays the experimentally determined CO_2 uptake of the CCR reactants as a function of their theoretical carbonation potential, both of which are expressed as a percentage of the reactant mass (i.e., g_{CO2}/g_r, where subscript 'r' indicates reactants). If the applied reaction conditions (and kinetics) were sufficient to achieve the theoretical carbonation potential during the experimental duration, all datapoints would lie along the "ideal carbonation" line (y = x). Such behavior may be observed when carbonation occurs in excess water, i.e., with high liquid-to-solid mass ratios, wherein reactant dissolution is maximized. However, in the experimental conditions employed, i.e., carbonation of dry reactant solids in contact with a humid gas stream (which is more relevant to cementation), the CO_2 uptake of all CCRs fell below the line of ideality, and a number of CCRs demonstrated effectively zero CO_2 uptake. For example, while fifteen CCRs demonstrated theoretical carbonation potentials greater than the 0.05 g_{CO2}/g_r performance threshold, only three CCRs demonstrated experimental CO_2 uptake greater than this threshold. These are CCR # 1, 9, and 19. Such ASTM C618 non-compliant CCRs that demonstrate relatively high CO_2 uptake are of special interest for the CO_2 mineralization process. However, CCRs that demonstrate low CO_2 uptake (and are calcium-poor) are also of interest for CO_2 mineralization processes,

as they promote pozzolanic reactions with $Ca(OH)_2$ that may improve later-age strength development in carbonated concrete mixture formulations.

Figure 3(b) displays the CO_2 uptake of the procured portlandite reactants, ascertained in a similar manner. The portlandite reactants also demonstrate sub-ideal CO_2 uptake, but achieve a greater fraction of their ideal CO_2 uptake than fly ashes and have higher uptake potentials. All grades of portlandite exceeded the 0.05 g_{CO2}/g_r criterion.

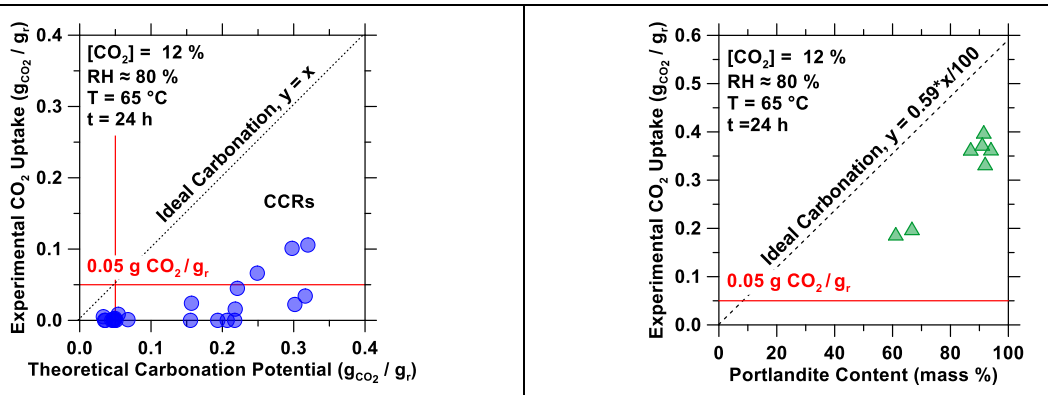

(a) **(b)**

Figure 3: The experimentally determined CO_2 uptake of **(a)** coal combustion residues (CCRs) as a function of their theoretical carbonation potential as determined by the Steinour equation, and **(b)** of hydrated lime reactants as a function of their purity (i.e., mass-based portlandite ($Ca(OH)_2$) content)). All experiments were performed in contact with a simulated flue gas stream containing 12 % CO_2 (v/v) at a relative humidity (RH) ≈ 80 % and T = 65 °C for a 24 h contact time (t).

3.2 Carbonation kinetics of reactants

The time-dependent CO_2 uptake of selected portlandite and CCR reactants were assessed experimentally using the custom-built bench-scale carbonation reactors described in the previous section (see Figure 2) using TGA. After equilibrating the powder samples to the proper relative humidity and temperature, using an inert gas stream for 30 minutes, CO_2 exposure was initiated for a total duration of 24 h. Triplicate powder specimens were extracted after CO_2 exposure durations of 1, 3, 7, and 24 h. Reactor conditions were maintained to T = 65 °C, RH ≈ 80 %, and $[CO_2]$ ≈ 12 % in each case. The purity of the portlandite particulates used varied from 92 % to 98 % (± 2 %) (by mass) with the remainder being composed of $CaCO_3$ as determined by TGA. The variations in portlandite purity were accounted for in calculating the portlandite conversion.

Figure 4(a) displays the time-dependent CO_2 uptake of portlandite reactants of four various grades: (a) reagent grade (Fisher Scientific), (b) Microcal HS, (c) Microcal HF, and (d) Standard hydrated lime (b-d sourced from Mississippi Lime Co). The equation $X(t) = (X_f \cdot t)/(X_f/k + t)$ (Eq. 1)[20] was fitted to the data to estimate the final (i.e., plateau) conversion X_f [fraction], and the apparent rate constant of carbonation k [s^{-1}].[20] The fitting was performed using the linearized form of Eq. 1 ($y = mx + b$) where the slope $m = 1/k$ and the y-intercept $b = 1/X_f$ (Figure 4b). The apparent carbonation rate constants thus determined varied from $k = 2.3 \times 10^{-4}$ s^{-1} to $k = 8.2 \times 10^{-4}$ s^{-1}, an approximate 3.6× increase in reaction

kinetics with varying portlandite grades. The rate constants were noted to slightly decrease with increasing reaction duration, which is indicative of the attenuating influence of reaction extent on the reaction rate.[21,22] However, to simplify the analysis, the use of a single apparent rate constant provided a sufficiently strong fit to the experimental conversion data. The sub-ideal final conversion (i.e., $X_f < 1$) observed for all reactants was adequately described by Eq. 1 and varied with portlandite grade. This is notable in that the conversion itself accounts for compositional influences on the potential CO_2 uptake. The differences in the final conversion of portlandite particulates were thought to be attributed to their surface area, which is correlated to their reported particle sizes. Indeed, the final conversion of the portlandite grades within this study (and sourced from a review of the literature)[23,24] indeed decreased as the reported median particle diameter (d_{50}) increased (Figure 4c). The CO_2 uptake potential of various portlandite reactants may be therefore established by consideration of both theoretical carbonation potential (a function of composition) and the particle size distribution (a physical characteristic).

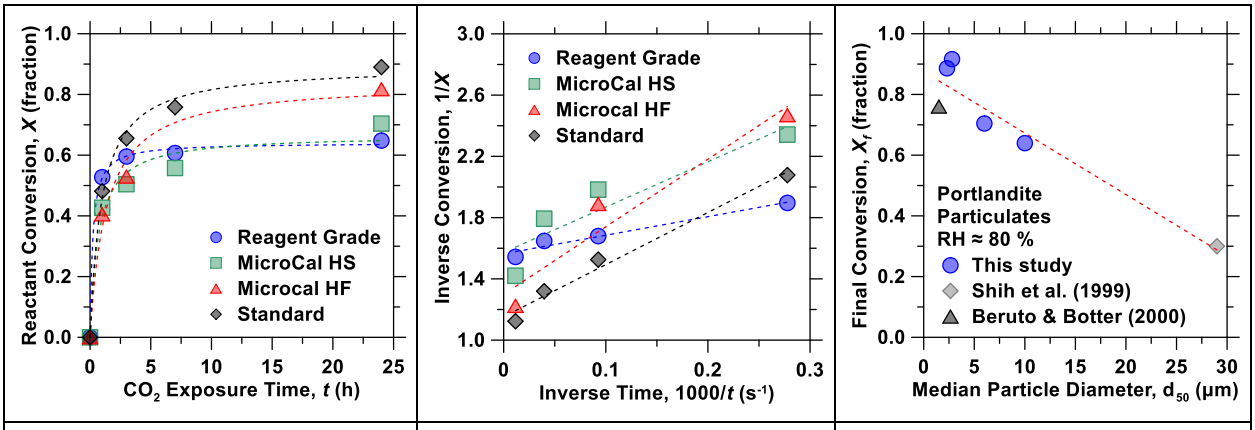

(a) **(b)** **(c)**

Figure 4: (a) The conversion-time curves describing the carbonation kinetics of four grades of portlandite particulates, assessed in contact with a simulated flue gas stream of T = 65 °C, RH ≈ 80 %, $[CO_2]$ = 12 %. The curve fits are of the form of Eq. 1. **(b)** The inverse conversion-inverse time profiles of portlandite particulate carbonation under the same reaction conditions. The linear curve fits displayed correspond to the linearized form of Eq. 1, where the slope $m = 1/k$ and the y-intercept $b = 1/X_f$. **(c)** A comparison of the final conversion X_f of the various portlandite grades in this study and two results from available literature data,[23,24] in relation to their reported median particle diameter (d_{50}).

The CO_2 uptake of three CCRs which demonstrated amongst the highest CO_2 uptake at 24 h (CCR # 1, 9, and 19) was similarly evaluated as a function of time (Figure 5a). Notably, the CO_2 uptake was approximately similar at all reaction times (assessed between 1 – 24 h of CO_2 exposure). All the (limited) CO_2 uptake within the selected CCR particulates occurred within the first 1 h of CO_2 exposure. Assessment of the inverse conversion-inverse time trends (Figure 5b) was therefore unable to reveal the apparent carbonation rate constants of the CCRs due to limitations in the experimental sampling. However, the results demonstrate that the CO_2 uptake of the CCRs may be assumed to be nearly instantaneous compared to the CO_2 exposure period.

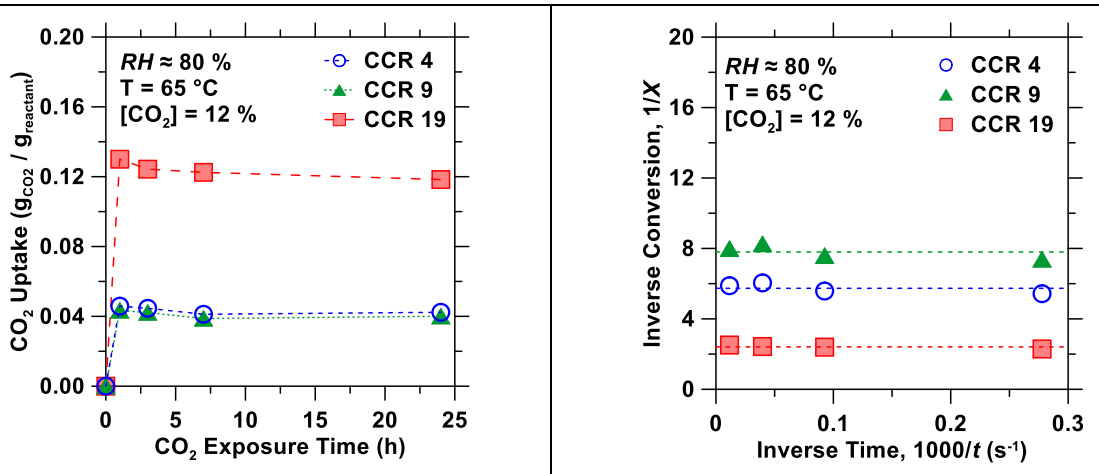

Figure 5: (a) Time-dependent CO_2 uptake **(b)** Inverse conversion-inverse time profiles of coal combustion residue (CCR) particulates during carbonation under the same reaction conditions. The linear curve fits displayed correspond to the linearized form of Eq. 1, where the slope $m = 1/k$ and the y-intercept $b = 1/X_f$. No reaction rate constant could be assessed due to the similarity in conversion values at all sampling time points (after 1 h CO_2 exposure).

3.3 Component performance

The carbonation kinetics of mixtures of portlandite particulates with either fly ash or OPC particulates were first evaluated. Figure 6(a) displays the 24-h CO_2 uptake of these mixtures as a function of the mass fraction of portlandite initially provided within the mixture. With the exception of slightly higher CO_2 uptake within OPC-containing mixtures, all mixtures demonstrated effectively similar CO_2 uptake, i.e., following a linear rule of mixtures controlled by the portlandite mass fraction. Therefore, it is expected that hydraulic/pozzolanic reactions between portlandite and fly ash (or within the OPC) exert limited influence on the CO_2 uptake of mixtures of particulates, in which the only water present is that adsorbed from a humid gas stream. The portlandite mass fraction is therefore the primary determinant of CO_2 uptake in such cases.

Based on these findings, a portlandite-enriched binder was formulated using: 42 mass % portlandite, 33 mass % ASTM C150-compliant[25] ordinary Portland cement (Type II/V OPC) and 25 mass % calcium-poor [26] fly ash (FA). OPC was incorporated to provide green strength and to facilitate handling prior to drying and carbonation, whereas FA served as a source of aluminosilicates to promote pozzolanic reactions. This mixture formulation is expected to provide intermediate CO_2 uptake, while provisioning sufficient quantities of OPC and FA to promote strengthening by hydraulic and pozzolanic reactions. The binder was combined with ASTM C33[27] compliant silica sand (fine aggregate) to form composites ("mortars") as described in ASTM C305.[28] Dry-cast composites were prepared with w/b = 0.25 (w/b = water-to-binder mass ratio) and a/b = 7.95 (a/b = aggregate-to-binder mass ratio). The fine aggregate had a density of 2650 kg/m^3 and a water absorption[29] of ≤ 1.0 mass. Dry-cast composites were prepared by compaction

using a hydraulic press to form cylindrical specimens (75 mm × 40 mm; $d \times h$). The compaction pressure was varied between 0.5 MPa and 22.0 MPa to achieve relative densities (ρ/ρ_s, the ratio of bulk density to skeletal density) ranging between 0.58-to-0.88, which also altered the initial saturation of pores with water (S_w). The initial S_w of cementitious components is an influential parameter to CO_2 transport, and therefore strongly alters the CO_2 uptake (Figure 6b). For example, reducing S_w from 0.53 to 0.32 in dry-cast composite increased the CO_2 uptake by ≈ 36 % after 60 h CO_2 exposure, but further reduction in S_w to 0.03 reduced the CO_2 uptake by ≈ 82 %.

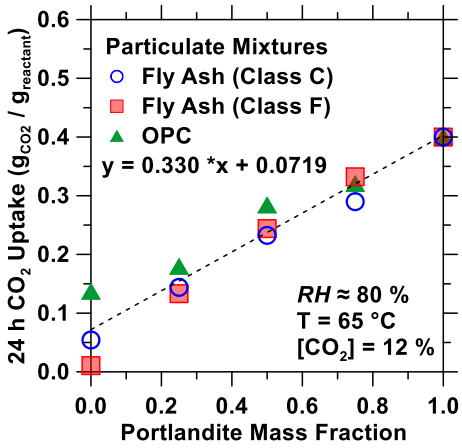

(a)

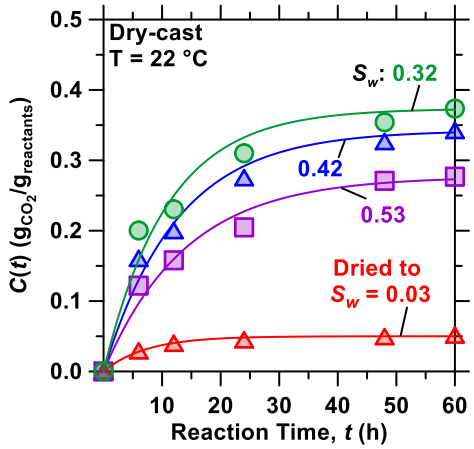

(b)

Figure 6: (a) The 24-h CO_2 uptake of mixtures of portlandite particulates with either fly ash or OPC particulates. **(b)** The time-dependent CO_2 uptake within dry-cast composites at varying initial saturation S_w. The data was fit by an equation of the form $C(t) = C(t_u)[1 - \exp((-kt)/C(t_u))]$ to estimate the apparent carbonation rate constant. The initial saturation in dry-cast cementing formulations is an important parameter that influences the CO_2 uptake, which must be maintained above a critical value ($S_{w,c}$ ≈ 0.1) to promote carbonation. In (b), carbonation was carried out using 12 % CO_2 [v/v] at 22 °C.

The compressive strength of the composites was measured as per ASTM C39.[30] Appropriate strength correction factors were applied in consideration of the specimens' length-to-diameter ratios.[30] The strength of the dry-cast composites increased with S_w (Figure 7a), for various reaction extents/degrees of CO_2 uptake. However, this is, in part an artifact resulting from the reduction in total porosity that resulted from the increased levels of compaction that were used to elevate S_w. For example, analytical analysis of particle packing[31] within the dry-cast composites reveals a 4× reduction in the interparticle spacing as the relative density increased from 0.67 to 0.88. Not only does this improve particle-to-particle contacts, but it also permits more effective cohesion in the material by a smaller quantity of cementing agent (carbonate precipitates). Carbonation of the dry cast composites at room temperature provided up to ≈ 12 MPa compressive strength immediately following CO_2 exposure, which is less than the performance threshold relevant to load-bearing concrete masonry products (e.g., compressive strength > 13.8 MPa, ASTM C90). However, the required compressive strength of 13.8 MPa is required at a specimen age of 28

days. The compressive strength of the carbonated concrete mixtures may therefore be increased to meet ASTM C90 requirements by (1) further curing, e.g., commonly performed under submersion in saturated limewater or under water-misted burlap, or (2) by processing at higher temperatures to promote hydration and pozzolanic reactions of OPC and fly ash particulates within the processing period.

As noted in Figure 7(b), elevating the reaction temperature substantially enhanced both CO_2 uptake and strength, resulting in the development of $\sigma_c \approx 25$ MPa in 24 h; substantially exceeding the product standard in an accelerated production timeline. This is attributed to both facilitated CO_2 transport due to the removal of water by evaporation (increased carbonation reaction rate), and the stimulation of OPC hydration and pozzolanic reactions (as indicated by w_n/m_{OPC} in Figure 7b). However, in agreement with the results for drying-induced changes in S_w, a temperature increase is beneficial to a limit – further increasing the temperature to 85 °C diminished both CO_2 uptake and strength gain on account of the insufficiency of pore water to support both CO_2 mineralization and OPC hydration reactions. This is attributed to: (a) the exothermic nature of carbonation reactions wherein temperature rise (unless the heat is rapidly dissipated) shifts the reaction equilibrium towards the reactants thereby resulting in a retardation in reaction progress; following Le Chatelier's principle, and (b) the rapid extraction of water, as a result of which carbonation and hydration are both suppressed due to the rapid decrease in the liquid saturation level in the pores. These observations suggest that use of a partially humidified CO_2 (flue gas) stream could favor carbonation in composites having low water contents (e.g., dry-cast composites) that are processed at higher temperatures. As an example, the flue gas emitted from a coal-fired power plant typically features temperatures (T) and water vapor contents (w_v, v/v) on the order of 50 °C ≤ T ≤ 140 °C and 12 % ≤ w_v ≤ 16 %, respectively.[32,33] The water vapor present in the flue gas could thus compensate for that loss due to evaporation at such high temperatures.

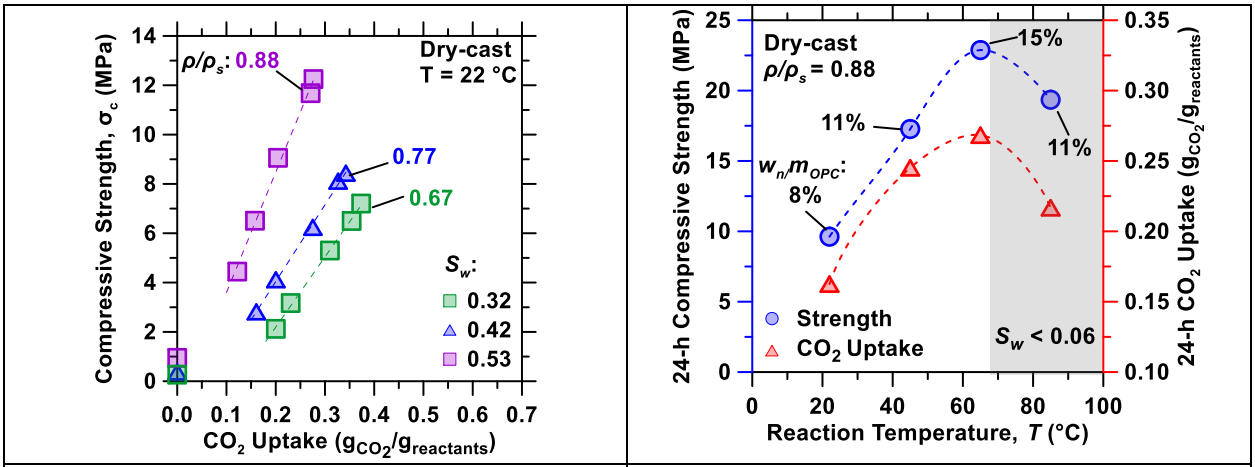

Figure 7: (a) The evolution of compressive strength as a function of CO_2 uptake for dry-cast composites at varying initial saturation levels induced by compaction pressure. **(b)** The evolution of 24-h compressive strength and CO_2 uptake as a function of the reaction temperature for dry-cast composites. Herein, carbonation was carried out using 12 % CO_2 [v/v].

4 Task 3.0 – Bench-scale studies to acquire critical data for system design

The Stonemaker DM100 block machine was selected to fulfill the project needs for production of blocks for prototype testing. Figure 8 presents photographs of the DM100 system, as installed at UCLA. The DM100 performs mixing, loading, and block forming actions – hydraulically powered – controlled by a solid-state digital control panel (Figure 8a). Fresh concrete mixtures (containing the cementing binder, aggregate, and water) are batched and homogenized in a 48" diameter pan mixer (Figure 8b). The mixing container is raised hydraulically to drop the homogenized concrete mixture into a hopper. The hopper then feeds the material into the block mold (Figure 8b), which forms up to three 8" x 8" x 16" standard hollow-core concrete masonry units simultaneously. The top section of the mold compacts the blocks into shape by hydraulic compaction and vibration. The resulting blocks – i.e., fresh dry-cast concrete masonry units, or "green bodies" – are loaded on plywood pallets and ejected on a track for off-loading (Figure 8c). The fresh blocks are then cured or carbonated after forming.

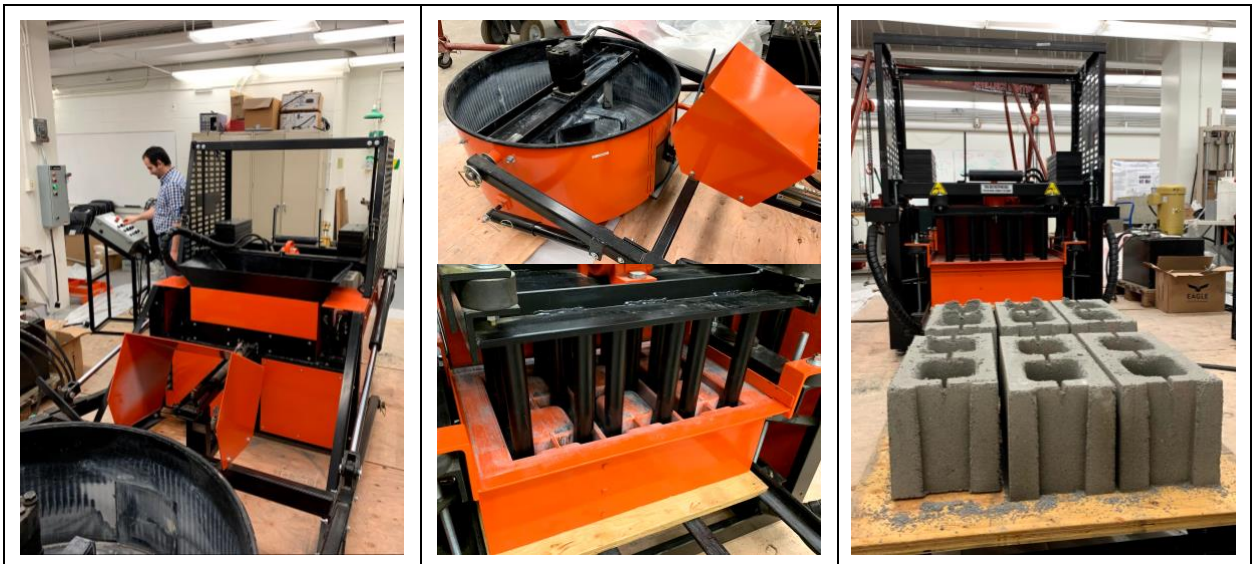

(a)	(b)	(c)

Figure 8: Photographs of the Stonemaker DM100 system as installed and operationalized at UCLA for production of prototype carbonated concrete masonry units, including **(a)** a view of the block-making system including control panel, **(b)** the pan-style mixer and mold/press, and **(c)** a view from the product offload track, depicting freshly produced carbonated concrete masonry units.

Additionally, a bench-scale reactor for carbonation experiments utilizing full-scale concrete blocks was fabricated. Figure 9 displays a schematic and photographs of the bench-scale carbonation system, which includes gas mixing equipment, a humidification chamber, a reaction chamber, and associated instrumentation. The reactor system simulates flue gas compositions of varying CO_2 concentration, relative humidity, temperature, flow rates and flow directions. CO_2 and air are mixed to appropriate concentrations by controlling their flow rates via mass flow controllers (MFCs). The mixed (dry) gas is then humidified by passing it through a heated vessel into which water is fed at a fixed rate via a syringe pump

and vaporized. Alternatively, the gas stream may be passed through a gas washing bottle for humidification. The humidified gas stream passes into the reaction chamber, which is formed from a heat-taped and insulated stainless steel batch can. The reaction chamber holds a single concrete block, which is instrumented for temperature. Temperature, relative humidity, and CO_2 concentration of the gas stream at the reactor inlet and outlets are measured via appropriate instrumentation (i.e., thermocouples, RH sensors, and a gas chromatograph). This instrumentation enables calculation of the balances of water and carbon dioxide entering/leaving the concrete block over the course of the CO_2 exposure.

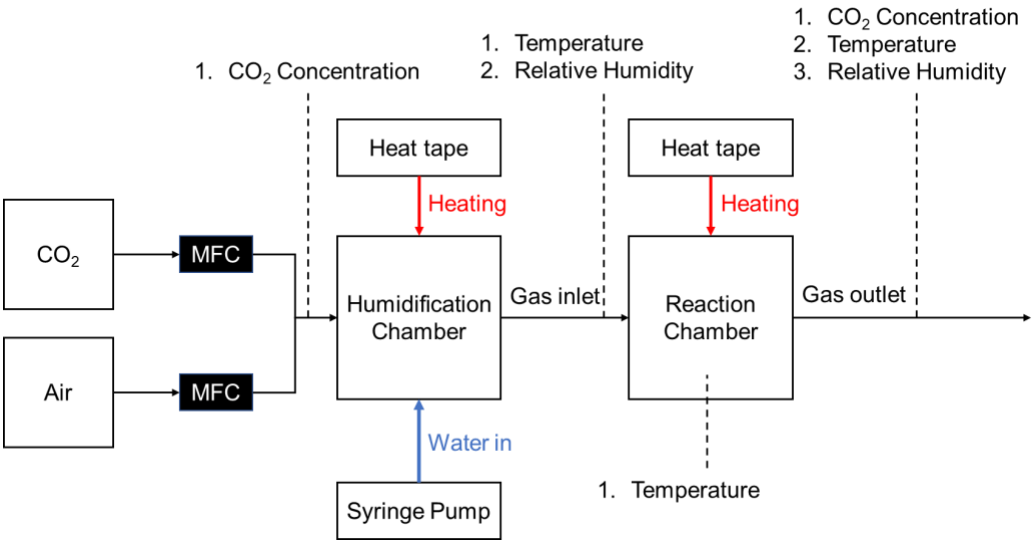

(a)

(b)

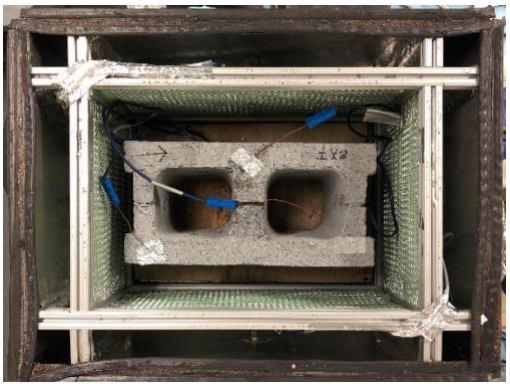

(c)

Figure 9: (a) Schematic and **(b-c)** photographs of the bench-scale reactor system and instrumentation used for carbonation experiments of concrete masonry units produced using the Stonemaker DM100.

The process conditions and the investigated ranges are described in Table 4. The inlet flow directions are described schematically in Figure 10. The CO_2 uptake within the carbonated concrete block was assessed using TGA. At the relevant time, the block was removed from the reactor and samples were extracted using a rotary hammer drill. Representative samples (at least 100 g) were taken from each side (long dimension), each face (short dimension), and the web (i.e., the interior wall between the two hollow cores). The CO_2 uptake measured within each sample was normalized by the initial mass of reactants within the mixture, where reactants refers to the sum of portlandite (CH, 42 mass %), Portland cement (OPC, 33 mass %), and Class F fly ash (FA, 25 mass %). To describe the CO_2 uptake within each block, wherein carbonation may not be uniform at all sampling locations, the "overall CO_2 uptake" within block was estimated as a volume-weighted average based on the sampled locations:

$$Overall\ CO_2\ uptake\ (g_{CO2}/g_{reactants}) = \sum C(24h)_i\ (g_{CO2}/g_{reactants}) \times v_i \qquad \textbf{(Eq. 2)}$$

where $C(24h)_i$ is the 24-h CO_2 uptake of section i of the concrete block (i.e., side, face, or web) and v_i refers to the volume fraction of that section in relation to the entire block volume.

Table 4: A experimental matrix for carbonation kinetics studies of concrete block. Unless specified, all experiments were carried out at: [CO_2] = 12.7% v/v.

Process parameters / Mixture formulation	***Objective:*** To determine the effects of temperature, relative humidity, gas flow direction, gas flow rate, pre-curing time, and presence of steam curing on carbonation kinetics					
	Temp-erature (T, °C)	Gas relative humidity (RH, %)	Inlet flow direction	Gas flow rate (F, slpm) (% CO_2 utilization)	R.T. pre-curing before CO_2 exposure (h)	Steam curing period before CO_2 exposure (h)
Baseline carbonated concrete mixture	33, 55, 71	20, 42, 60	longitudinal, transverse, both, top	1.23 (100), 2.45 (50), 4.92 (25)	12, 24, 48	12, 24

Longitudinal flow (LO) 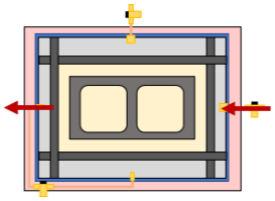	**Transverse flow (TR)** 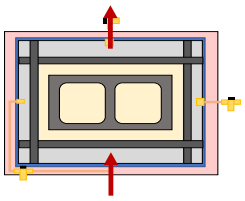
(a)	**(b)**
Both 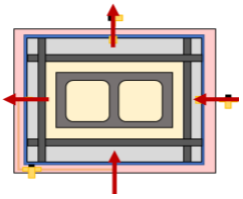	**Top flow (TOP)** 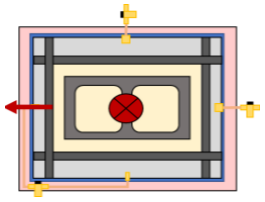
(c)	**(d)**

Figure 10: A schematic depicting the inlets and outlets of the simulated flue gas stream in the following configurations: **(a)** longitudinal flow, **(b)** transverse flow, **(c)** both longitudinal and transverse flows, and **(d)** top flow with side outlet. In all experiments, the concrete blocks were placed on solid plywood pallet within the reaction chamber.

Figure 11(a) displays representative time-dependent CO_2 uptake at the inlet face in the longitudinal flow configuration under varying *RH*. Reducing *RH* from 60 % to 20 % significantly increased both the reaction rate and the 24-h CO_2 uptake (Figure 11b). This is because the low gas relative humidity facilitated the removal of water (reducing the pore water saturation, S_w, Figure 11c). Following 24-h CO_2 exposure, S_w of the block varied from 0.59 (for *RH* = 60 %) to 0.16 (for *RH* = 20 %. These results indicate the importance of provisioning a processing environment that decreases S_w (even in dry-cast components) to enhance carbonation kinetics.

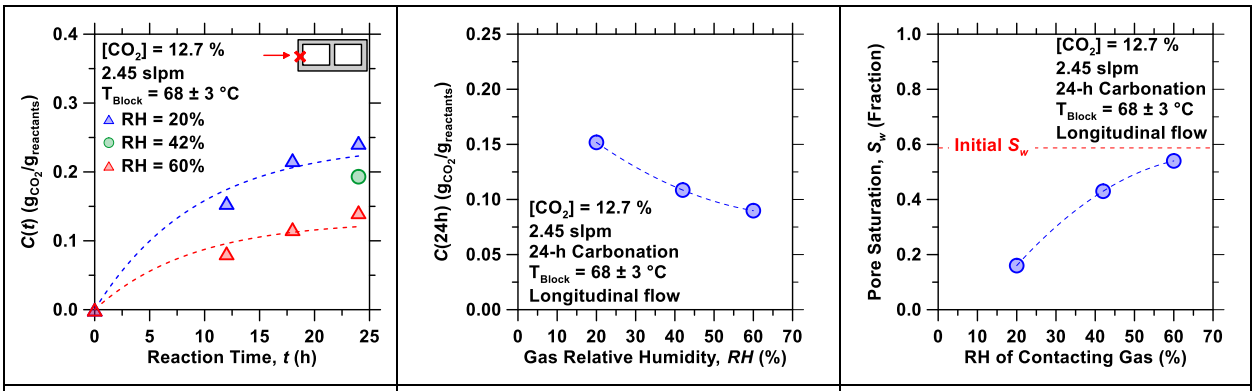

Figure 11: (a) The time-dependent CO_2 uptake within concrete block for varying gas relative humidity values at the inlet face in the longitudinal flow configuration. **(b)** The effects of *RH* on the **(b)** 24-h CO_2 uptake and **(c)** the pore saturation S_w of block following CO_2 exposure for 24 h. In **(b)**, the reported CO_2 uptake values represent the overall CO_2 uptake across entire block (all sections) as determined using Eq. (1). In all cases, blocks were pre-cured at 21 ± 1 °C for 12 h prior to CO_2 exposure.

Figure 12(a) displays representative time-dependent carbonation profiles indicating the effect of block temperature on carbonation kinetics, given a fixed *RH* ≈ 60 %. In this condition, elevating block temperature by heating the reactor only slightly enhanced CO_2 uptake, and with diminishing returns with further heating. Note, the difference in CO_2 uptake is the most significant at this sampling location (inlet face, longitudinal flow). Figure 12(a) shows the overall CO_2 uptake as a function of temperature, which portrays this overall weak dependence of carbonation extent on block temperature. On this basis, controlling *RH* is a more significant lever towards optimizing carbonation kinetics than is elevating gas temperature, within the investigated conditions.

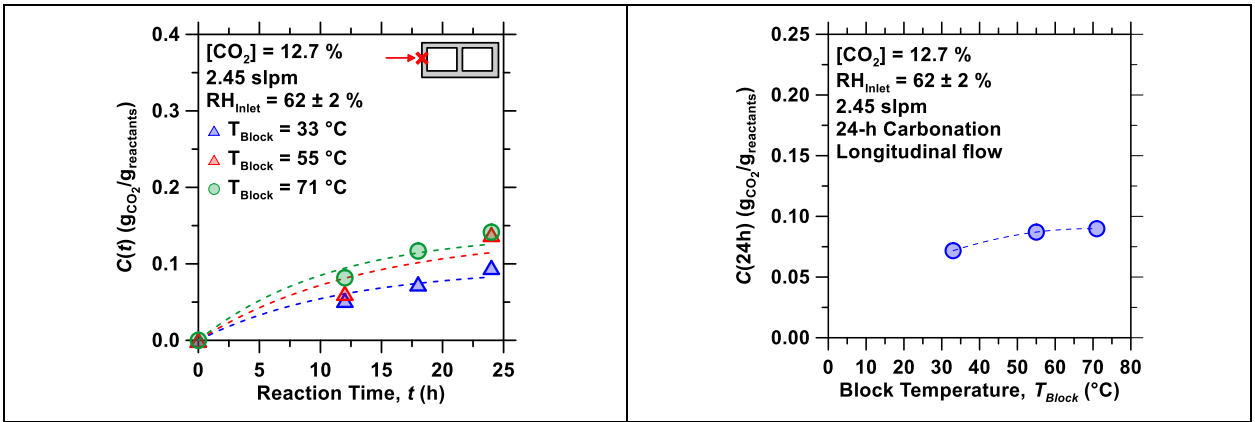

Figure 12: (a) The time-dependent CO_2 uptake within concrete block for varying block temperature values at the inlet face in the longitudinal flow configuration. **(b)** The effect of block temperature on overall 24-h CO_2 uptake determined using Eq. (2). In all cases, blocks were pre-cured at 21 ± 1 °C for 12 h prior to CO_2 exposure.

The four flow directions described in Figure 10 were compared under equivalent processing conditions, with the overall CO_2 uptake described in Figure 13. The gas flow distribution affects both the carbonation kinetics and the uniformity of CO_2 uptake across different block sampling locations. In the present reactor system, the "top flow" configuration produced the greatest and most uniform CO_2 uptake. The flow design in the reactor will seek to mimic these conditions. This may be achieved using flow distributors that direct the flue gas vertically, which will require porous (i.e., wire mesh) shelves to support the blocks. Alternatively, the blocks may be placed on their sides (i.e., hollow cores oriented horizontally) in alignment with a horizontally distributed gas flow.

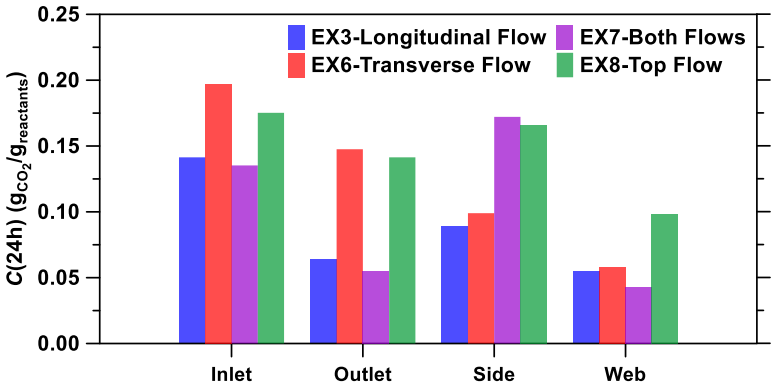

Figure 13: The CO_2 uptake within concrete block for varying inlet gas directions following 24-h CO_2 exposure. In all cases, blocks were pre-cured at 21 ± 1 °C for 12 h prior to CO_2 exposure.

Increasing the flow rate of simulated flue gas accelerated carbonation (Figure 14a), largely due to the increased rate of drying during carbonation. Doubling the flow rate from 1.23 slpm (a rate that provisions an amount of CO_2 that can achieve 100 % CO_2 utilization based on the theoretical CO_2 uptake capacity of the block) to 2.45 slpm (50 % CO_2 utilization) resulted in a 15 % increase in CO_2 uptake. However, further increasing flow rate yielded only 6 % higher CO_2 uptake. These results broadly indicate the efficacy of inputting a greater quantity of flue gas per unit time, which must be considered against the reduced theoretical maximum CO_2 utilization efficiency that may be realized, as the quantity of CO_2 input exceeds the uptake of the reactants.

As limitations in site logistics may require varying the time delay before blocks are imposed, it is expected that the duration of this delay (i.e., pre-curing time, in which the OPC within the carbonated concrete block may undergo hydration) may impact the carbonation kinetics. To investigate this effect, freshly formed concrete blocks were cured at room temperature, wrapped in plastic sheeting to minimize water evaporation, for varying durations prior to CO_2 exposure. Figure 14(b) displays the 24-h overall CO_2 uptake as a function of pre-curing time. Extending precuring time from 12 h to 48 h reduced the overall CO_2 uptake by 10 %. This effect can be linked to the further progression of OPC hydration during pre-curing, indicated by increased non-evaporable water content w_n quantified by TGA (Figure 14c). The increased extent of OPC hydration produces greater quantities of C-S-H precipitates within the material, which may hinder carbonation by imposing microstructural constraints to CO_2 transport, and covering (portlandite)

reactant surface area. However, as OPC hydration after the first 12 h curing is slow, the extent of carbonation is only weakly sensitive to the duration of pre-curing

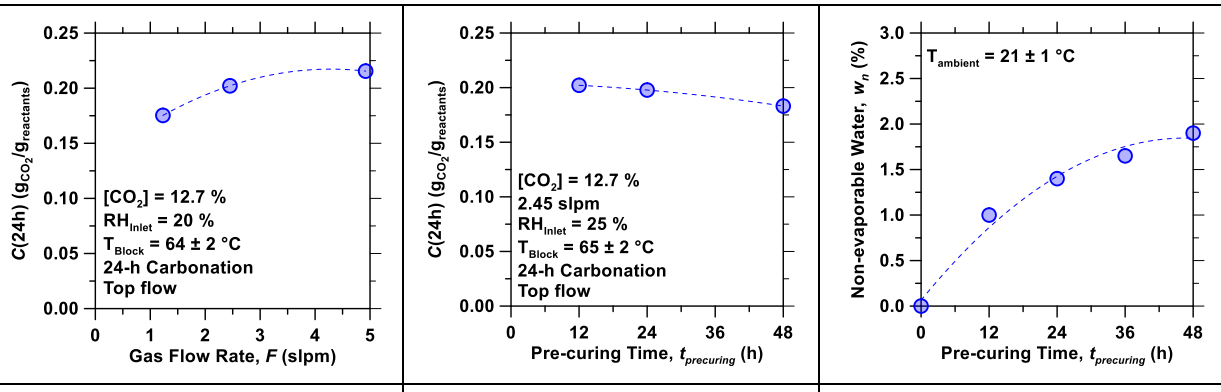

(a) **(b)** **(c)**

Figure 14: The effect of gas flow rate on the overall 24-h CO_2 uptake of the carbonated concrete block, and **(c)** pore saturation level S_w of block during CO_2 exposure. The blocks were pre-cured at 21 ± 1 °C for 12 h prior to CO_2 exposure. **(b)** The effects of pre-curing time on the overall 24-h CO_2 uptake of block during CO_2 exposure. **(c)** The evolution of non-evaporable water content w_n as a function of pre-curing time. During pre-curing blocks were covered with plastic sheet and maintained at 21 ± 1 °C prior to CO_2 exposure.

In summary, towards the objective of establishing process conditions that maximize the rate of CO_2 uptake in excess of 5.8 x 10^{-7} g CO_2 / g reactant / second, Figure 15 displays the overall CO_2 uptake rate for the various process conditions evaluated. It is noted that all evaluated conditions exceed the 5.8 x 10^{-7} g CO_2 / g reactant / second criterion, supporting the robustness of CO_2 uptake to variations in process conditions. It is further noted that the process conditions that produce optimal carbonation behavior are identified as *RH* = 20 % and reactor temperature ≈ 45 °C. These conditions balance water removal and hydration reaction progress. Increasing the gas flow rate accelerates drying, which enhances the carbonation rate (although with diminishing returns when increasing the flow rate above 2x). Increasing flow rate further increased CO_2 uptake, indicating the impact of increased superficial velocity within the reactor; however, this rate must be considered carefully in relation to the required CO_2 utilization efficiency of the system. Regarding flow direction, a "top-down" flow direction produced the greatest reaction rate (and most spatially-uniform carbonation extent) of all configurations tested. When these conditions are ensured, extending the pre-curing duration before CO_2 exposure reduced the CO_2 uptake only slightly. Alternatively, a process of simulated steam curing before CO_2 exposure, during which the block was exposed to heated, humid air, negatively impacted CO_2 uptake rates by increasing the saturation of the block's pore network. These findings inform the process conditions and steps (and therefore process design) that will optimize the CO_2 uptake rates achievable in the carbonated concrete mineralization system.

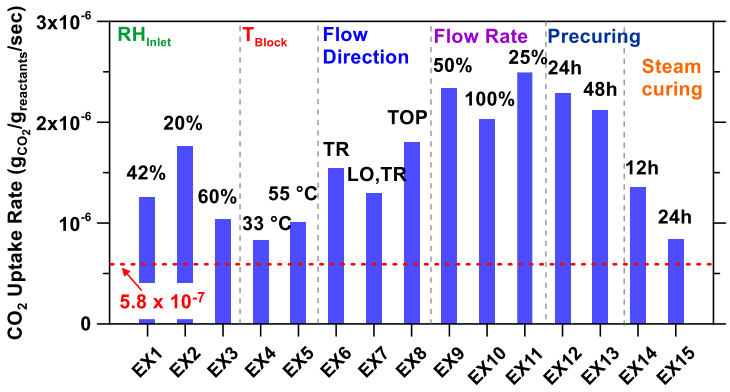

Figure 15: The overall CO_2 uptake rate (averaged over the 24-h CO_2 exposure duration) at different experimental conditions after 24 h CO_2 exposure. The horizontal line indicates a rate of 5.8×10^{-7} $g_{CO2}/g_{reactants}$ /second, which was the defined minimum criterion for the CO_2 uptake rate. Abbreviations: TR = Transverse flow; LO = Longitudinal flow; LO, TR = both; TOP = top flow. Simulated steam curing utilized air with flow rate of 0.5 slpm, T = 75 ± 5 °C and RH = 80 %. The simulated steam curing increased block temperature from 21 ± 1 °C to 27 ± 1 °C and it remained constant during steam curing period.

In parallel to the investigation of process conditions kinetics, a bench-scale reactor was configured to enable the investigation of the effects of acid gases on carbonation reaction kinetics (e.g., see Figure 16). Carbonation experiments were performed in simulated flue gas containing NO_2 and SO_2 in concentrations similar to the specified flue gas composition exiting the Wyoming ITC host site (i.e., containing 13 ppm NO_2, 21 ppm SO_2). Herein, due to the need for engineering controls (i.e., housing within a fume hood) in the event of gas leakage from the reactors, the system scale was reduced, necessitating the use of cylindrical mortar specimens (i.e., that contain paste, and fine aggregates; wherein the paste consists of portlandite, fly ash, cement and water). These samples were exposed to the aforementioned simulated flue gas streams containing acid gases, and a reference simulated flue gas of equivalent CO_2 concentration (without SO_2 and NO_2), in order to ascertain the influence of these gases on the rate of CO_2 uptake and development of mechanical properties (i.e., compressive strength). CO_2 exposure was performed for 24 h, after which the overall (total) CO_2 uptake was determined to be 0.0303 ± 0.0051 g of CO_2/g of mortar in the presence of acid gases, and 0.0286 ± 0.0020 g of CO_2/g of mortar, in the absence of acid gasses. As such, within experimental uncertainty, the presence of acid gases did not affect the rate of formation of carbonate solids. The compressive strength of the two materials similarly showed no dependence on the presence of acid gases. Samples carbonated in the presence of, and in the absence of NO_2 and SO_2 featured compressive strengths on the order of 6.11 ± 0.08 MPa and 5.79 ± 0.39 MPa, respectively. As such, it is clarified that the presence of NO_2 and SO_2 in the flue gas from coal-fired power plants will neither affect the CO_2 conversion efficiency, nor the mechanical properties of the carbonated concrete.

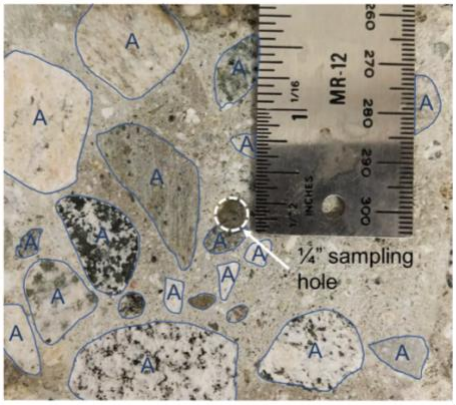

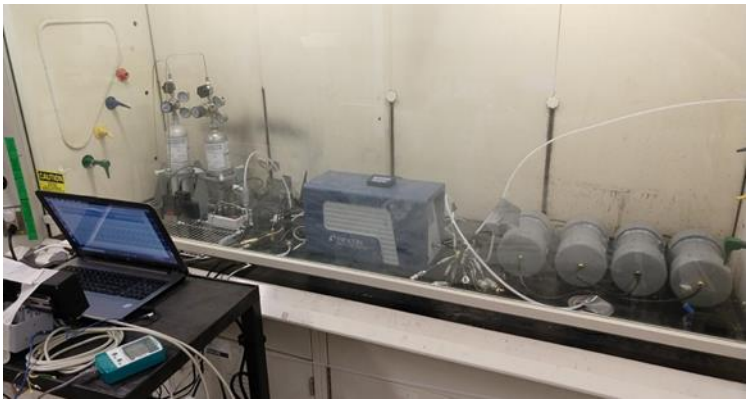

(a) **(b)**

Figure 16: (a) An illustration of the carbonated concrete composite surface which shows large aggregates outlined and marked as "A". Powder samples were extracted from the center of the cylindrical sample using a ¼" drill-bit for thermal analysis. **(b)** An illustration of the reactor system that was used to examine the progress of carbonation in the presence of "acid gases" (i.e., NO_2 and SO_2) within a fume hood.

4.1 Quantification of heat and mass transfer in the Reversa process

4.1.1 *Isothermal Calorimetry*

Isothermal calorimetry (TAM Air, TA Instruments) was performed on carbonated concrete mixture formulations (i.e., pastes and mortars) to quantify the heat generation by hydraulic and/or pozzolanic reactions immediately after material synthesis (i.e., mixing water, aggregate, and cementing binder) and in the absence of CO_2 exposure (beyond that of atmospheric CO_2). The eight mixtures listed in Table 5 were evaluated at three different isothermal temperatures: T = 25 °C, 45 °C, and 65 °C. These mixtures were developed to isolate the binary interactions between each of the binder components (i.e., OPC-CH, OPC-FA, FA-CH), and the effects of water-to-solids ratio (w/s) and the aggregate type on hydration kinetics. Following a standardized mixing procedure using an IKA 4-blade impeller-type mixer, ≈ 10 g of material was measured into glass ampoules and loaded into the calorimeter cells. The first 30 minutes of data were neglected due to the non-isothermal response that results from opening the cells/sample loading. The heat flow signal was normalized by the mass of cement (or binder) within the material, as noted.

Table 5: Cementitious mixtures evaluated by isothermal calorimetry.							
#	**Mixture**	**Cement, OPC (mass %)**	**Fly Ash, FA (mass %)**	**$Ca(OH)_2$, CH (mass %)**	**Water, w (mass %)**	**Quartz, Q (mass %)**	**Aggregate, A (mass %)**
1	OPC Paste	66.7	0	0	33.3	0	0
2	OPC-FA-Q	22	16.7	0	33.3	28	0
3	OPC-CH-Q	22	0	28	33.3	16.7	0
4	FA-CH-Q	0	16.7	28	33.3	22	0
5	OPC-FA-CH	22	16.7	28	33.3	0	0
6	OPC-FA-CH (w/b 0.2)	27.5	20.8	35	16.7	0	0
7	OPC-FA-CH-A (w/b 0.2)	5.0	3.8	6.4	3.0	0	81.7
8	OPC-FA-CH-Q (w/b 0.2)	5.0	3.8	6.4	3.0	81.7	0

Figure 17 displays the heat release profiles obtained by isothermal calorimetry for all tested mixture formulations. Figure 17a indicates the reactivity of a neat OPC paste (water-to-binder mass ratio, w/b =0.5), and the acceleration of OPC hydration that is achieved with increasing reaction temperature from T= 25 °C to 65 °C. Further, the heat release was used to estimate the time-dependent degree of OPC hydration θ(t) (fraction) as

$$\theta(t) = \frac{Q(t)}{C_b \Delta H_{hyd}} \quad \textbf{(Eq. 3)}$$

where $Q(t)$ is cumulative heat release as a function of time (J), C_b is the binder content (kg binder/kg specimen), and ΔH_{hyd} is the ultimate heat release due to OPC hydration, given by

$$\Delta H_{hyd} = m_{C_3S}\Delta H_{C_3S} + m_{C_2S}\Delta H_{C_2S} + m_{C_3A}\Delta H_{C_3A} + m_{C_4AF}\Delta H_{C_4AF} \quad \textbf{(Eq. 4)}$$

where m_i is the mass fraction of the i^{th} phase within the cement, and ΔH_i is its reaction enthalpy (J/g). The composition of the cement was estimated via XRF analysis provided by the supplier as 61.4 % C_3S, 12.8 % C_2S, 7.5 % C_3A and 8.5 % C_4AF, on a mass basis. The ΔH_i values were sourced from the literature.[34] Figure 18 displays the degree of hydration of the OPC paste (Mixture 1), assessed via isothermal calorimetry, as a function of the equivalent age (t_{eq}), which was calculated as

$$t_{eq} = \int_0^t \exp\left[-\frac{E_A^{hyd}}{R}\left(\frac{1}{T} - \frac{1}{T_{ref}}\right)\right] dt$$

(Eq. 5)

where R is the universal gas constant (8.314 J/mol·K), T is the absolute temperature (K), T_{ref} is a reference temperature (selected as 303.15 K), and E_A^{hyd} is the activation energy of hydration, determined as E_A^{hyd} = 38.5 kJ/mol. This value was selected by varying E_A^{hyd} until the degree of hydration curves in Figure 18 demonstrated the best fit to a single master curve (i.e., strongest overlap). This activation energy and master curve are used as input into the finite element model described in the following section.

The heat release profiles of Figure 17 provide further insight into the impacts of each binder component onto hydration heat. For example, while Mixture 5 represents the standard ternary carbonated concrete binder, Mixture 2, 3, and 4 represent binders each missing one of the binder components, i.e., calcium hydroxide, fly ash, and OPC, respectively. Comparing the calorimetry response of these mixtures suggest that the presence of calcium hydroxide had little influence on the heat release of the binder, while including fly ash caused a substantial increase. This may suggest that the reaction heat is increased by (1) the hydration of fly ash itself, (2) the pozzolanic reaction of fly ash with calcium hydroxide, or (3) acceleratory effects of fly ash on OPC hydration, i.e., filler effects. Of these explanations, (3) may be the most significant, because the fly ash used was silica-rich (Class F), and the heat release of its pozzolanic reaction was small within the evaluated testing duration (see Figure 17d). Further, comparison of Figure 17e and Figure 17f indicates that reducing w/b (i.e., from a wet-cast to dry-cast mixture) reduces the heat release by approximately one-third.

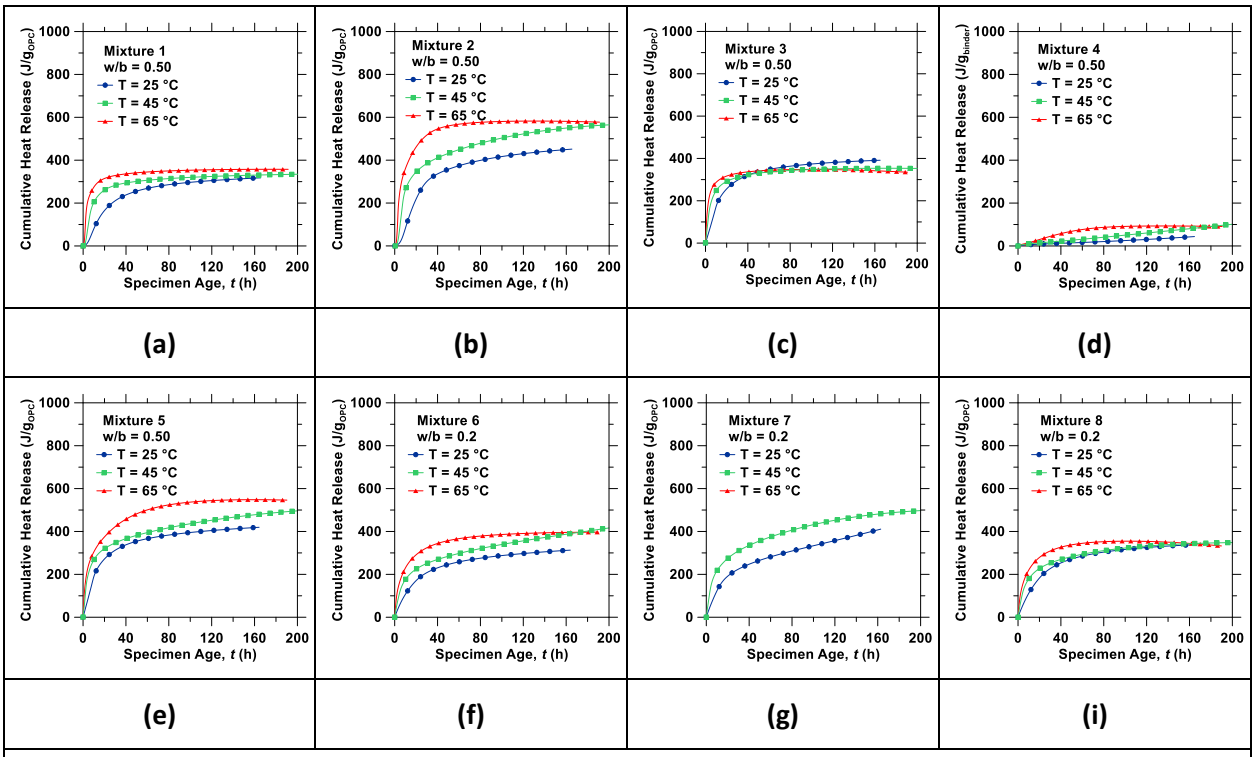

Figure 17: (a-i) Isothermal calorimetry heat release profiles from Mixtures 1-8. All profiles are normalized by the mass of OPC within the specimen except for Mixture 4 (FA-CH-Q), which contains no OPC and was therefore normalized by the total binder mass.

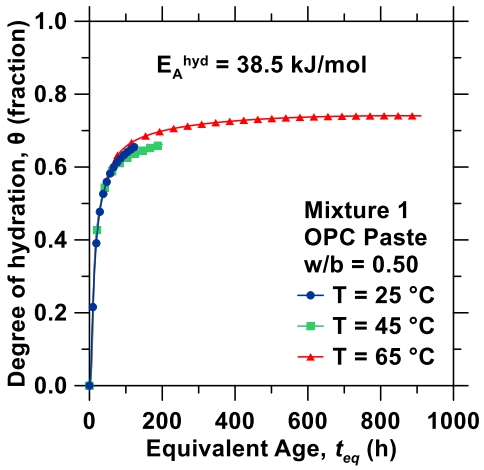

Figure 18: The degree of OPC hydration θ as a function of the equivalent age t_{eq} as calculated using Eq. 4. The plots here are the final curves evaluated using the "best-fit" activation energy of cement hydration indicated on the figure.

4.1.2 *Model Formulation, Geometry, and Assumptions*

During the carbonation processing of carbonated concrete, several reactions occur concurrently, including: (1) the carbonation reaction of portlandite, (2) hydration of Portland cement, (3) pozzolanic reactions between fly ash and portlandite, (4) carbonation reactions of Portland cement phases and hydrated cement phases, and (5) vaporization/condensation of pore water (physical).

As a preliminary basis, it is assumed that the primary phenomena of interest are (1, 2, 5), and that reactions (3) and (4) are negligibly influencing heat and mass transport within carbonated concrete processing. In the initial model formulation, it is assumed that transport within the dry-cast carbonated concrete block is governed by diffusion only (i.e., zero velocity field and zero convective transport of liquid or vapor in the material). Rather than considering each elementary reaction step, (i.e., dissolution of $Ca(OH)_2$ and CO_2 and precipitation of $CaCO_3$), the model considers an overall portlandite carbonation reaction. As such, this model formulation ignores the transport of CO_2 that is dissolved within pore water, i.e., as CO_2, HCO_3^- and CO_3^{2-}. This choice is justified by prior experimental findings, i.e, that carbonation of mortars is negligible in cases wherein the mixtures are nearly completely saturated with water, and by the fact that CO_2 diffusion in liquid is approximately 10,000 times slower than in gases.

Under the aforementioned assumptions, a one-dimensional finite element model was developed within COMSOL to describe heat and mass transfer in carbonated concrete specimens. Figure 19 illustrates this 1-D domain with its relevant boundary conditions. An abbreviated description of the model follows.

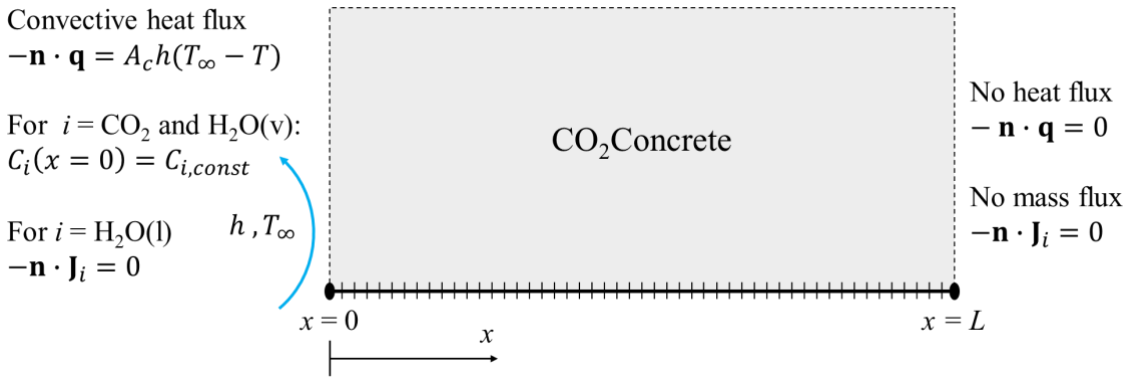

Figure 19: A schematic of the one-dimensional simulation domain representing the cross section of a carbonated concrete block, with thickness *L*. The boundary conditions for heat and mass transfer at both boundaries are also described in the figure.

4.1.3 *Governing Equations – Mass Transfer*

Within the carbonated concrete domain, the concentration of each species "i" c_i (mol/m^3), that is, CO_2 (gas), H_2O (liquid) and H_2O (vapor), is governed by

$$\frac{\partial c_i}{\partial t} + \nabla \cdot \mathbf{J}_i = R_i \quad \textbf{(Eq. 6)}$$

where D_i is the diffusion coefficient (m^2/s), $\mathbf{J}_i$ is the diffusive flux ($mol/m^2 \cdot s$) equivalent to $\mathbf{J}_i = (-D_i \nabla c_i)$ and R_i is the reaction rate ($mol/m^3 \cdot s$). The effective diffusion coefficients of each species within the porous medium of carbonated concrete are described as

$$D_{H_2O,v}^{eff} = D_{H_2O,v-air}(T)\phi^{4/3}S_g^{10/3} \quad \textbf{(Eq. 7)}$$

$$D_{CO_2,g}^{eff} = D_{CO_2-air}(T)\phi^{4/3}S_g^{10/3} \quad \textbf{(Eq. 8)}$$

where ϕ is the total porosity (volume fraction), S_g is the saturation of the pores with gas (fraction) i.e., $S_g + S_l = 1$ where S_l is the saturation of the pores with liquid water. $D_{i-air}(T)$ is the temperature-dependent free diffusion coefficient of the i^{th} species, which is described by an Arrhenius relation

$$D_{i-air}(T) = D_{i-air}^0 \exp\left(-\frac{E_{A,i-air}}{RT}\right) \quad \textbf{(Eq. 9)}$$

where R is the gas constant (8.314 J/mol·K), $D_{CO_2-air}^0 = 2.16 \times 10^{-4}\ \mathrm{m^2/s}$, $D_{H_2O-air}^0 = 3.56 \times 10^{-4}\ \mathrm{m^2/s}$, and $E_{A,CO_2-air} \approx E_{A,H_2O-air} = 6.5\ \mathrm{kJ/mol}$, estimated by fitting data tabulated by Cussler (2009).[35] The transport of liquid water was described by the relation

$$D_{H_2O,l}^{eff} = 2.3 \times 10^{-13} \exp(9.95\phi) S_l^3 \quad \textbf{(Eq. 10)}$$

which has been previously demonstrated to describe the transport of liquid water in porous cementitious materials.[36] The reaction rate of liquid water is the sum of reaction rates due to vaporization of liquid water (i.e., producing water vapor), OPC hydration which consumes water to produce calcium silicate hydrate (C-S-H) gel and calcium hydroxide, and portlandite carbonation, which releases liquid water

$$R_{H_2O,l} = -m_{H_2O,l}^{vap} - m_{H_2O,l}^{hyd} + m_{H_2O,l}^{carb} \quad \textbf{(Eq. 11)}$$

$$m_{H_2O,l}^{vap} = k_{vap}\left(a_w \cdot c_{H_2O,v}^{sat} - c_{H_2O,v}\right) \quad \textbf{(Eq. 12)}$$

where k_{vap} is the rate constant of evaporation (s^{-1}), $c_{H_2O,v}$ is the current concentration of water vapor $c_{H_2O,v}^{sat}$ is the water vapor concentration at saturation, which is a function of the local temperature and pressure. The reaction rates of water due to hydration and carbonation are handled using COMSOL's chemical reaction module based on an assumed reaction stoichiometry and rate constants, which require validation.

4.1.4 *Governing Equations – Heat Transfer*

The temperature (T) of the porous carbonated concrete medium is governed by the equation

$$A_c\left(\rho C_p\right)_{eff}\frac{\partial T}{\partial t} + \nabla \cdot (-A_c k_{\mathrm{eff}} \nabla T) = A_c Q \quad \textbf{(Eq. 13)}$$

where A_c is the cross-sectional area (fixed as 1 m^2), ρ is the density of the medium (kg/m^3), C_p is the heat capacity (J/ g·K), and k_{eff} is the effective thermal conductivity of the composite (W/m·K). The effective thermal properties of the medium were calculated as

$$\left(\rho C_p\right)_{eff} = \phi_p \rho_p C_{p,p} + \left(1 - \phi_p\right)\rho C_p \quad \textbf{(Eq. 14)}$$

$$k_{eff} = \phi_p k_p + (1 - \phi_p)k + k_{disp} \quad \textbf{(Eq. 15)}$$

where the thermal properties of the porous medium were assumed as constants. The thermal properties of the air inside the pores were modeled as humid air, using built-in properties within COMSOL. The volumetric heat generation Q (W/m^3) was described as the sum of heat generation resulting from: (1) OPC hydration (assessed via isothermal calorimetry), (2) portlandite carbonation as described the reaction stoichiometry, and (3) the vaporization of liquid pore water, that is

$$Q = Q_{vap} + Q_{hyd} + Q_{carb} \quad \textbf{(Eq. 16)}$$

The heat of vaporization was simply related to the rate of vaporization by

$$Q_{vap} = -\Delta H_{vap} \cdot Mn_l \cdot m_{H_2O,l}^{vap} \quad \textbf{(Eq. 17)}$$

where ΔH_{vap} is the enthalpy of vaporization of liquid water (i.e., 2.45×10^6 J/kg), $Mn_{H2O,l}$ is the molecular weight of water (i.e, 18.015 g/mol), and $m_{H_2O,l}^{vap}$ is the rate of vaporization described previously. The heat of carbonation was similarly described as

$$Q_{carb} = \Delta H_{carb} \cdot m_{carb} \quad \textbf{(Eq. 18)}$$

Finally, the heat of OPC hydration was described as

$$Q_{hyd} = \frac{C_b \Delta H_{hyd}\, \theta_\infty B}{t_{eq}} \left(\frac{\tau}{t_{eq}}\right)^B \times \exp\left[\left(\frac{\tau}{t_{eq}}\right)^B\right] \times \exp\left[-\frac{E_A^{hyd}}{R}\left(\frac{1}{T} - \frac{1}{T_{ref}}\right)\right] \quad \textbf{(Eq. 19)}$$

where θ_∞, B and τ are fitting constants in the equation best fit to the data in Figure 17.

$$\theta(t_{eq}) = \theta_\infty \exp\left[-\left(\frac{\tau}{t_{eq}}\right)^B\right] \quad \textbf{(Eq. 20)}$$

The equivalent age was solved for as a function of depth and time within the carbonated concrete specimens in the differential form

$$\frac{\partial t_{eq}}{\partial t} = \exp\left[-\frac{E_a}{R}\left(\frac{1}{T(x,t)} - \frac{1}{T_{ref}}\right)\right] \quad \textbf{(Eq. 21)}$$

These calculations were necessary for calculating the mass balances and process flow diagrams used for the design and fabrication of the concrete carbonation reactor.

5 Task 4.0 – Design and fabrication of modular CO_2 processing system

5.1 Component selection and system design

Details for this section were sent to DOE in a quarterly report during the course of the project. These details were not included in this report as they would contain proprietary and confidential information.

5.2 System construction

Based on the design basis described above, the project team's bid package was competitively-bid to multiple firms for the completion of system design and fabrication. As a result of this competitive bidding process, AirClean Technologies was identified as the lowest qualified bidder on the process, and was therefore selected as the project team's partner for the completion of engineering design and fabrication. AirClean provided a refined process flow diagram (PFD), building upon the preliminary PFD in the DBM, piping and instrumentation diagrams (P&IDs), and equipment lists and specifications necessary to define all process equipment in detail. Following the equipment specification, a general arrangement was developed, which includes all necessary gas processing equipment on a modular skid, in addition to the modular shipping container which was housed in a 40' open-side shipping container at the ITC and outside for the NCCC demo. Following detailed design, hazard analysis, and approvals, AirClean procured the equipment and materials necessary for system fabrication and assembled the modular process equipment within their facility. The completed process skid and curing chamber underwent factory acceptance testing, following which they packed and transported to the Wyoming ITC host site for integration in the flue gas slipstream and subsequent operations. AirClean has qualified and dedicated engineering and fabrication staff capable of performing these tasks, with significant experience in similar modular process equipment in the energy sector.

An internal P&ID review meeting was convened at AirClean's office in Kennesaw, GA on 1/10/2020. The agenda of the meeting is reproduced below in Table 6.

Table 6: Agenda for Internal P&ID review meeting.

Time	**Description**	**Required Attendees**
10:15 am – 11:00 pm	P&ID Review	UCLA/AirClean
11:00 am – 12:00 pm	P&ID Walkthrough with DOE and NCCC team	UCLA/AirClean /DOE/NCCC
12:00 pm – 2:00 pm	Working Lunch - Review Acid Dew Point Temperature - Discuss Insulation Specification and Heat Loss Calculation - Discuss Hydraulic Calculation - Discuss General Arrangement - Review Control Narrative Discuss Inlet/Outlet Nozzle Design	UCLA/AirClean
2:00 pm – 2:30 pm	Review Questionnaire from ITC	UCLA/AirClean
2:30 pm – 3:30 pm	Call with George Laird at Predictive Engineering re: CFD results and design	UCLA/AirClean/ Predictive
3:30 pm – 4:00 pm	Review QA Manual	UCLA/AirClean
4:00 pm – 4:15 pm	Review Project Management Documents	UCLA/AirClean
4:15 pm until end	Mark Up P&IDs for HAZOP	UCLA

Participants included Gabriel Falzone (UCLA), Iman Mehdipour (UCLA; remote), Ben Gardner (consultant), Tony Wu (National Carbon Capture Center (NCCC; remote), Dave Cerotzke (AirClean), Max Reichlin (AirClean; remote), Bill Hunter (AirClean; remote) Andrew Jones (DOE; remote), and George Laird (Predictive Engineering; remote). Tony Wu of NCCC provided comments on the design documents relevant to installation and operations at the NCCC site. The major outcomes of this meeting included: editorial corrections to the design documents, first investigation into operating curing chamber under slight negative pressure to reduce risk of flue gas leakage into enclosure, removal of heater that was installed immediately upstream of exhaust stack, refinement of control narrative relating to control of recycle ratio, identification of necessary revisions to GA, and further discussion to finalize design of chamber gas flow distribution system via CFD analyses. The design changes identified during this meeting were addressed prior to the HAZOP review meeting that followed in January.

The fabrication of the CO_2 mineralization system was completed, including the curing chamber and process skid. Figure 20 displays photographs of the curing chamber during various stages of the project.

(a) **(b)**

Figure 20: (a) Photographs of the CO_2 mineralization curing chamber during fabrication at AirClean's shop **(b)** Curing chamber as delivered to storage in Gillette, Wyoming.

Before shipment of the system to Gillette, WY, factory acceptance tests (FATs) were completed. A FAT report has been prepared that lists all inspection notes, punch list items, and their rectification, and data logged during the extended 24 h FAT using heated air.

6 Task 5.0 – Commissioning and trial operation of the Reversa process

6.1 System start-up/commissioning

6.1.1 *Convened remote HAZOP review meeting with relevant stakeholders for ITC host site, and identify requirements for ITC installation*

A Hazard and Operability (HAZOP) Review meeting was convened at the Wyoming ITC on 01/24/2020. Attendees included: Gabe Falzone (UCLA), Iman Mehdipour (UCLA), Ben Gardner (HAZOP facilitator), Will Morris (Wyoming ITC), Ray DeStefano (Wyoming ITC), Jim Ford (Wyoming ITC), Tony Wu (NCCC), Tim Hansen (350 Solutions), Dave Cerotzke (AirClean), Max Reichlin (AirClean), and Andrew Jones (DOE). The P&ID was systematically reviewed for risks in the case of events including: high flow, low flow, high pressure, low pressure, vacuum, reverse flow, loss of power, high level, low level, high flow, and low flow. The impact of each event, and the current action/safeguard against it was identified. Each event was then scored in terms of probability, cost impact, schedule impact, and safety risk, using the scoring criteria described in Table 7. The total rating of each event was given a rating calculated as the probability score times the sum of cost, schedule, and safety risk scores. Recommended actions to mitigate these risks were identified and addressed in the final system design or by Standard Operating Procedures where necessary. An updated HAZOP report reflecting the as-built conditions was submitted to DOE, indicated the mitigation of risks following the design modifications.

Table 7: HAZOP scoring criteria used in 1/24/20 HAZOP meeting at Wyoming ITC.	
PROBABILITY RANKING	
Nearly impossible (less than once a year event)	1
Remote chance (once a year event)	2
Occasional (more than once a year event)	3
Reasonably possible (once a month event)	4
Frequent, inevitable (more than once a month event)	5
COST RANKING	
< $1000	1
$1000 ≤ $10,000	2
≥ $10,000	3
SCHEDULE IMPACT RANKING	
≤ 1 DAY	1
1 DAY ≤ 7DAYS	2
≥ 7 DAYS	3
SAFETY RISK	
NO CHANCE OF INJURY	1
CHANCE OF MINOR INJURY	2
CHANCE OF MAJOR INJURY	3
CATASTROPHIC, COULD RESULT IN FATALITY	4

6.1.2 *Convened remote HAZOP review meeting with relevant stakeholders for NCCC host site, and identify requirements for NCCC installation*

A remote HAZOP review meeting with NCCC stakeholders was completed on 5/27/2020. A HAZOP report was generated, containing the following action items to be completed before system installation at the NCCC:

1. Add to the SOP checklist to close V002 during a power loss event.

2. Consider adding glycol to chiller water line as additional freeze protection measure.
3. Consider adding insulation to chiller water lines since chiller unit will be outside.
4. Verify that humidification water lines are insulated
5. Calculate temperature of discharge water from P-104
6. Add a low point drain to humidification water line
7. Add to the SOP to close V005 and V006 during power outage
8. Consider adding period humidification nozzle inspections to SOPs
9. Add insulation to water drain lines and relief lines
10. Add water drain lines and relief lines to freeze protection SOP
11. Add water trap inspection to rounds and readings
12. Verify that the CO_2 analyzer vent lines are discharged to safe location (i.e. 14 ft above unit or point down to grade).
13. Verify that the CO_2 analyzer isolation valves are closed when not in use
14. Consider checking CO_2 analyzer lines and draining after runs during winter

These action items were addressed. The team also provided to the NCCC additional information that was requested to facilitate their design process, including additional equipment and instrument specifications, electrical schematics, etc.

6.2 Startup and commissioning

Following system installation at the ITC, and the approval of ITC host site staff following the system walkdown inspection, startup and commissioning activities were performed. Issues identified and corrected during startup and commissioning included:

1. Leaks in threaded connections in chiller water line [corrected by removing connections and applying additional sealant]
2. Improper function of chiller water control valve (TCV-004) [corrected by altering control valve wiring connections]
3. Incorrect calculation of flow rates in PLC [PLC program was modified to properly adjust flow calculations]
4. Recycle line flow rate inconsistent with mass balance [replaced Dwyer pitot tube with spare, flow rate now consistent]
5. Insufficient control of flue gas inlet and recycle control valve positions [modified PLC to allow for fixed positioning of control valve positions]
6. Issue in CO_2 analyzer datalogging timing [corrected via modifications to PLC program]
7. CO_2 analyzer sample pump insufficient to overcome negative pressure in chamber outlet line [CO_2 sampling point moved to recycle line; auxiliary vacuum pumps to be provided]

Further, the commissioning activities at ITC and NCCC verified that the system's instrumentation properly measures the mass balances across the curing chamber. Commissioning trials were also used to define the valve positions and fan settings required to achieve the desired system gas flow rates while maintaining a slightly negative pressure in the curing chamber (to prevent flue gas leakage from the chamber into the enclosure.

A walkdown inspection was conducted at the NCCC but no alterations were required as all changes from the HAZOP were completed.

7 Task 6.0 – Field demonstration of Reversa carbonation system

7.1 Host site preparation

7.1.1 *Host-site preparation for ITC*

Concrete footings for the curing chamber (Figure 21a) and process skid (Figure 21b) were installed on the ITC site in Small Bay B, which has been assigned to the team for testing. A temporary steel enclosure was delivered to the ITC to protect the system from the elements (Figure 21c).

(a)

(b)

(c)

Figure 21: ITC site preparation photographs including **(a)** concrete strip footings featuring gravel backfill and insulation panels for curing chamber, **(b)** concrete footings for process skid, and **(c)** steel enclosure delivered to Wyoming ITC site to be assembled around system once installed.

The team completed the required tenant agreement with the Wyoming ITC, and was assigned to “Small Bay B” for testing.

7.1.2 *Host-site preparation for NCCC*

Following the NCCC HAZOP, significant preparations were made for the NCCC demonstration, including the following:

- Completed follow-up actions identified in NCCC HAZOP
    - Procured foam rubber insulation for drain lines on skid to prevent freezing
    - Removed condensate drain lines from curing chamber to wastewater reservoir and sealed ports. These drain lines were not effective as minimal water condensation was observed within the curing chamber.
    - Installed low point drain on humidification water loop to be used in event of freezing temperatures.
    - Procured glycol-based antifreeze mixture for use in chilled water loop as a replacement of water to prevent freezing in cold weather.
    - Modified standard operating procedures to include draining water lines in freeze protection scenario and closing flue gas valve in loss of power scenario
- Provided system delivery and storage guide to NCCC
- Provided additional design details and scope of work to NCCC for installation
- Completed the NCCC’s Technology Screening Form
- Completed NCCC host site agreement

Following completion of the first field demonstration at Wyoming ITC, the system was delivered to NCCC site at the end of November 2020 for the second field demonstration. Figure 22 presents photographs of the system in various stages of installation. The primary installation steps were performed as follows:

1. Install curing chamber and skid onto foundations
2. Install chamber-skid connecting piping
3. Install return flue gas lines from system to host site
4. Connect system flue gas inlet to site flue gas header
5. Connect system water inlet to site water supply
6. Install electrical panels and tie in to supply panel
7. Install building lighting and heaters (LV panel)
8. Connect system to site electrical (HV panel)
9. Install air-cooled water chiller and tie-in water line to system
10. Install instrumentation tubing lines
11. Install system insulation for pipes using foam insulation
12. Install P-traps and drain lines for curing chamber
13. Install internal gas flow distributors

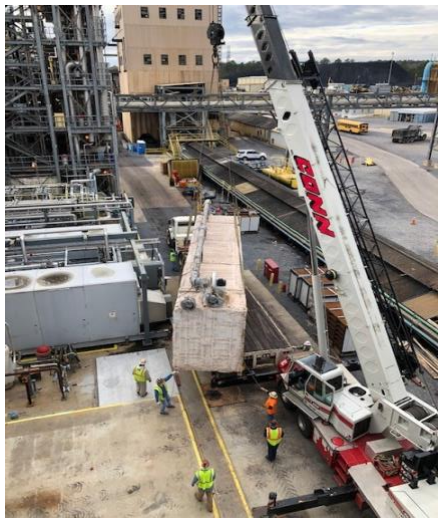

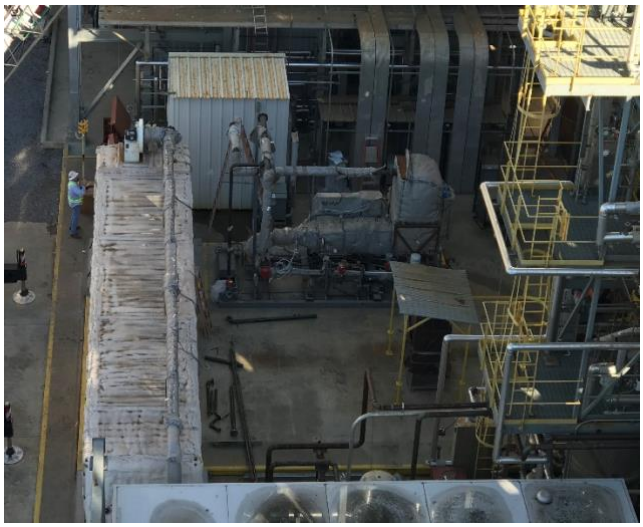

(a) **(b)**

Figure 22: Photographs of **(a)** delivery of curing chamber, and **(b)** the CO_2 mineralization curing chamber and process skid installed onto their foundations.

7.2 Test plan development

7.2.1 *Refined test plan, operations and HSE manual for ITC operations*

The test plan for operations at the Wyoming ITC was completed (see Table 8). The plan included the overall number of operational batches (11), their expected durations, and whether they are performed continuously (back-to-back) or with built-in lag between batches to allow for modifications.

Table 8: Test plan schedule table for ITC demonstration.

Phase	Batch #	Production at TCC	Interval (d)	ITC delivery	Delivery time
Phase A (Weekly basis)	A1	7/8/20	7	7/9/20	Before 12 pm
	A2	7/15/20	7	7/16/20	Before 12 pm
	A3	7/22/20	7	7/23/20	Before 12 pm
	A4	7/29/20	7	7/30/20	Before 12 pm
	A5	8/5/20	7	8/6/20	Before 12 pm
Phase B (Continuous basis)	B1	8/13/20	8	8/14/20	Before 12 pm
	B2	8/19/20	6	8/20/20	Before 12 pm
	B3	8/26/20	7	8/27/20	Before 12 pm
	B4	9/2/20	7	9/3/20	Before 12 pm
	B5	9/10/20	8	9/11/20	Before 12 pm
	B6	9/16/20	6	9/17/20	Before 12 pm

Operations and HSE manuals for ITC operations were compiled, comprising:

- System standard operating procedures
- Shutdown procedures
- Cold weather shutdown procedures
- Rounds and readings checklists
- Lock-out tag-out procedures
- Materials safety datasheets
- Environmental permitting requirements
- Management of change procedure

7.2.2 *Refined test plan, operations and HSE manual for NCCC operations*

The main objectives of the pilot-scale demonstration of the carbonated concrete mineralization system at NCCC site in Wilsonville, AL were as follows:

- Refine the process following the ITC demonstration to optimize system performance and system energy input,
- Demonstrate robustness with respect to flue gas CO_2 concentration (coal: 10-13 vol% and NG: 4-9 vol%) and environmental conditions,
- Utilize high-volume of coal combustion products (CCPs) in carbonated concrete block formulations (>25 mass %),
- Develop a code compliance report in collaboration with the International Code Council's Evaluation Service (ICC-ES) for carbonated concrete products.

Following installation and commissioning, the carbonated concrete system was demonstrated over 6 operational runs at the NCCC to produce structural CMUs. The UCLA team partnered with Blair Block in Childersburg, AL to produce concrete blocks using the carbonated concrete formulations. Each operational run consists of the following steps (see Figure 23):

- Concrete block production (using the carbonated concrete formulation) at Blair Block manufacturing facility in Childersburg, AL,
- Concrete block "semi-curing" at Blair Block to gain sufficient *green-strength* for transportation,
- Truck Transportation of the palletized concrete blocks to NCCC,
- Weighing and loading of concrete blocks into the carbonation chamber,
- Applying the Reversa processing including: drying, carbonation, humidification, and,
- Unloading, palletizing, sampling, and performance testing of the concrete blocks.

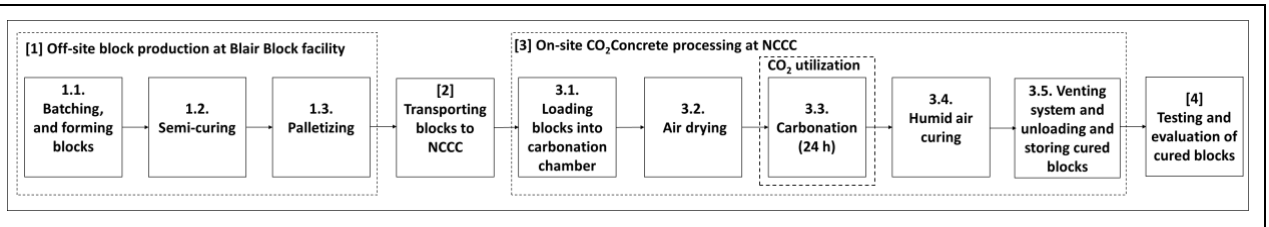

Figure 23: The steps involved in the Reversa process cycle to produce concrete blocks including both off-site (at Blair Block facility) and on-site (at NCCC site) activities.

Table 9 presents the test plan for 6 demonstration runs and system processing.

Table 9: Test plan and operational procedures for Reversa demonstration at the NCCC site.

Batch #	Flue gas source (CO_2 %)	Carbonation duration	Milestone description
N1	Coal (~12 vol%)	18 hours	**Objective: Baseline without gas processing** • Effect of highest RH on CO_2 uptake without any gas processing
N2	Coal (~12 vol%)		**Objective: System process** • Effect of RH control on CO_2 uptake • Effect of RH control on system energy demand
N3	Coal (~12 vol%)		
N4	NG (~4 vol%)		**Objective: CO_2 concentration** • Effect of CO_2 dilution on CO_2 uptake and product performance • Control of space velocity of curing chamber
N5	NG (~4 vol%)		
N6	Coal (~12 vol%)		**Objective: Material formulation** • Effect of cement formulation on product performance and CO_2 uptake

7.3 Installation and operation

7.3.1 *System measurement and verification plan*

The system's measurement and verification plan is summarized below.

7.3.1.1 Process overview

The carbonated concrete block production process incorporates the following steps (see Figure 23 in Section 7.2.2): **[1]** At a concrete block plant, concrete mixtures are batched from their raw materials (i.e., aggregates, binders, and water) and homogenized. This mixture is subsequently compacted using a concrete block machine to form fresh, shape-stabilized concrete blocks. **[2]** The semi-cured concrete blocks are then transported from the block manufacturing plant to the demonstration site, **[3]** where they are loaded into a curing chamber for the following sequential processing steps: air-drying, flue gas injection and carbonation/CO_2 mineralization, and finally moist-curing. The cured carbonated concrete

blocks will then be removed from the curing chamber and stored. **[4]** The fully cured blocks will then be sampled and selected per a pre-determined scheme for off-site testing and evaluation of products.

The UCLA team identified TCC Materials, a concrete masonry producer in Rapid City, South Dakota which is in the closest proximity (≈ 2 h by road) to the Wyoming Integrated Test Center (ITC). TCC Materials has the capability to supply materials, form, pre-cure, palletize, and deliver semi-cured carbonated concrete blocks to the ITC host site for carbonation processing. Blair Block in Childersburg, AL, was the CMU supplier for the NCCC demonstration.

Once received on-site, each batch of carbonated concrete will be produced over an 80-h period which includes the following processing steps: (1) drying process, (2) carbonation process (i.e., a 24-h long continuous flue gas injection step), and (3) moist-curing process. The detail of the single operation cycle is as follows for the ITC demonstration:

- On day 1, upon delivery of semi-cured carbonated concrete blocks from TCC Materials to ITC site, the blocks will be manually loaded into 8 steel racks.
- The loaded racks will be transferred into the curing chamber using a forklift.
- The process cycle will initiate on day 1 and includes the following steps:
    - Drying with exposure to dry air
    - Carbonation with continuous flue gas injection
    - Moist-curing with exposure to moisture saturated air
- On day 3, the curing chamber will be vented of residual flue gas and the racks unloaded from the curing chamber using the forklift.
- On day 3, the finished carbonated concrete blocks will be manually unloaded, palletized, wrapped with a plastic sheet, and stored at the storage area until transportation.

The detail of the single operation cycle is as follows for the NCCC demonstration:

- On day 1, upon delivery of semi-cured carbonated concrete blocks from Blair Block to NCCC site, the blocks will be manually loaded into 8 steel racks.
- The loaded racks will be transferred into the curing chamber using a forklift.
- The process cycle will initiate on day 1 and includes the following steps:
    - Drying with exposure to dry air
    - Carbonation with continuous flue gas injection
- On day 2, the curing chamber will be vented of residual flue gas and the racks unloaded from the curing chamber using the forklift.
- On day 2, the finished carbonated concrete blocks will be manually unloaded, palletized, wrapped with a plastic sheet, and stored at the storage area until transportation.

Following a predetermined sampling scheme, fully cured blocks will be selected for evaluation of their CO_2 content and compressive strength.

7.3.1.2 Off-site operations at block manufacturing plant

For demonstration operations at the Wyoming ITC, the UCLA team has contracted TCC Materials, a concrete masonry producer in Rapid City, SD, to provide blocks composed to a specified formulation. The summary of the process flow at the TCC facility is described in Table 10, alongside the data recorded during each step, and the method of its measurement. A similar process flow was repeated by Blair Block for the NCCC demonstration.

Table 10: A summary of process steps and data generation and recording through off-site operations at the block manufacturing plant (TCC Materials). Steps repeated at NCCC demonstration.				
#	**Step**	**Data recorded during step**	**Method of measurement**	**Method of recording**
1.A	Raw materials (e.g., aggregate, fly ash, cement, portlandite, and water) are batched	Batch weights of all material inputs (except hydrated lime)	Online instrumentation in batching system	Printout of batch receipt
		Batch weights of hydrated lime	Visual Count	Hand-recorded on batch receipt
1.B	Block making machine forms concrete blocks into shape	Estimated power consumption; number of blocks formed; recording of excess material waste	Counting number of cycles	Hand-recorded in production log
1.C	Concrete blocks are moved to the curing room at T = 22 °C ± 2 °C for 12 h (this time may subject to change) to achieve sufficient *green-strength*	Temperature and time of pre-curing	Data-logging thermocouple in curing chamber	Automatic recording in logger, to be transferred to computer and plotted in production log
1.D	QC check and removal/disposal of sub-standard blocks during conveyance to cubing station	Weight of material removed (waste).	Balance	Recorded in production log
1.E	Concrete blocks are palletized (45 ea. pallet)	Number of blocks and pallets to be delivered to site	Visual count	Recorded in production log
1.F	Pallets are then loaded into an insulated shipping container to transport blocks to the ITC site	Confirmation of number of blocks and pallets shipped	Visual count	Bill of lading

This procedure will provide information to quantify the energy consumption of block production, and the material balance at the production site (i.e., input into the mixer, wasted in the form of defective blocks or excess material, and successfully formed into sound blocks).

7.3.1.3 Transportation of blocks to host site

The blocks will be transported from the block producers to the host sites. Table 11 describes the data to be recorded during transportation and the method of its measurement and recording.

Table 11: A summary of process steps and data generation and recording during transportation of blocks from block manufacturer (TCC Materials) to Wyoming ITC host site. Steps repeated at NCCC demonstration.

#	Step	Data recorded during step	Method of measurement	Method of recording
2.A	Transportation of blocks in trailer from TCC Materials to ITC host site	Duration and distance of route	Recording by driver	Delivery receipt
		Temperature of blocks within trailer	Data-logging thermocouple in curing chamber	Automatic recording in logger, to be transferred to on-site staff with delivery receipt
2.B	Delivery inspection and off-loading of blocks at the ITC host site	Observation of block quantity and condition upon arrival	Visual inspection and visual count	Delivery receipt

The duration and distance of the route will be used to estimate the consumption of diesel fuel (and direct emissions resulting from combustion) for the trailer that delivers the blocks to the host site. It should be noted that in a commercial production scenario, the block production system will be co-located at the emissions source, and therefore emissions and inputs related to this intermediate transportation scope would not be generated. Our LCA calculations will therefore be the production scenario as-is, and wherein this intermediate transportation scope of emissions is excluded.

7.3.1.4 Block handling and loading into curing chamber

Once on site, the concrete blocks are removed from the shipping container and are loaded into 8 steel racks for placement in the curing chamber. It should be noted that the initial CO_2 contents that are present in the aggregates and binders will be subtracted from the overall CO_2 uptake measured during the carbonation process to eliminate their influences on the CO_2 conversion achieved during carbonation and to offer a baseline for the CO_2 uptake calculation. Table 12 summarizes the relevant steps related to on-site block storage, handling, and loading into the curing chamber.

Table 12: An overview of process steps and data generation and recording during on-site block handling at the Wyoming ITC host site.				
#	**Step**	**Data recorded during step**	**Method of measurement**	**Method of recording**
3.A	On-site storage of palletized blocks	Duration of storage before loading into curing chamber	Difference between delivery time and loading time	Each pallet will be labeled with batch ID and number
		Storage temperature	Thermocouple logger	Logger data transferred to PC
3.B	Unloading palletized blocks into racks	Weigh the selected 72 test specimens following selection scheme	Balance and visual count	Hand-recording
3.C	Thermal analysis of selected pre-cured blocks	Initial CO_2 contents of five pre-cured blocks that are randomly selected from different pallets upon delivery	Thermogravimetric analysis (TGA)	Automatic recording of TGA traces in .txt file; recording of processed data using MATLAB and Excel spreadsheets
3.D	Loading racks of blocks into curing chamber	Total number of blocks loaded into curing chamber;	Visual inspection/count of blocks on each rack, and number of racks loaded	Record and photographs of loaded racks within reactor
		Time of loading	Clock	Hand record in storage log

7.3.1.5 Verification

The primary means of verification of the measurements will be using factory-calibrated measurement systems and field calibration after installation and commissioning. However, additional verification of performance will be provided because the collected measurements result in overspecification (known values exceed unknown variables) for the heat and mass balances. This approach allows calculation of the performance using multiple variable sets. With multiple variable sets for each balance, multiple estimations of the different variables will be possible. Therefore, poor or faulty measurements of any single (and possibly multiple) measurement systems do not adversely affect the ability to evaluate performance.

7.3.1.6 Data Management

Material inputs and outputs and energy consumption were closely monitored during operations (i.e., during forming, palletizing, delivery, before and after processing, and palletizing steps of finished carbonated concrete blocks), in order to verify production throughput and to tabulate the mass and energy balances. A data acquisition system was used to collect and store the process and performance measurements obtained from online instrumentation. The collection frequency for these data were between one and ten minutes.

7.3.1.7 Unloading and sampling of fully cured carbonated concrete blocks for characterization

The finished carbonated concrete blocks were manually removed from the racks by material handlers. As the blocks were being removed from the racks, test specimens were selected and labeled. To obtain an average CO_2 uptake and strength of the cured blocks, representative of the entire curing chamber, test specimens were selected from different shelves of each rack. As a result, 60 test specimens overall were selected for each production run. The mass of these selected 60 test specimens were recorded prior to and after completion of processing to determine the overall mass change of the carbonated concrete blocks. The selected units were sound and free from cracks upon visual inspection. If the block in the selected location does not fulfill this criterion, an adjacent block was selected, and the difference noted.

Table 14 summarizes the steps during block unloading and sampling.

Table 14: A summary of process steps and data generation and recording during block handling and sampling of fully-cured blocks produced after completion of every operation at Wyoming ITC host site.

#	Step	Data recorded during step	Method of measurement	Method of recording
4.A	Unloading racks of blocks from curing chamber	None	N/A	N/A
4.B	Manually removing blocks from racks	None	N/A	N/A
4.C	Selection and labeling of blocks for testing	Mass of selected blocks following sampling scheme	Balance	Manual recording of each block mass
4.D	Palletizing or disposing of excess blocks	None	N/A	N/A

7.3.1.8 CO_2 content and compressive strength of fully cured carbonated concrete blocks

Half of the selected blocks were used for compressive strength testing while the other half were tested for their CO_2 content using TGA. The reactor's symmetry was exploited to ensure that blocks with equivalent processing histories were tested in each method. To accurately determine the CO_2 content for block samples, several critical issues were considered and properly addressed. First, the concrete block should be sampled strategically so that the average CO_2 content for a given specimen geometry can be

reconstructed properly. For sampling, a rotary hammer provided with a 6 mm drill bit was used to extract powder samples from four surfaces of each carbonated concrete block (see Figure 24). In total, 12 powdered samples were taken across varying surfaces of the concrete block as indicated by red points in Figure 24. The extracted powders are then mixed to create a representative sample of the entire concrete block. After the CO_2 content is determined for the selected blocks across varying locations of racks and curing chamber, the overall CO_2 content was averaged based on the mass proportions for each section to properly reconstruct the average conversion level of all blocks within the curing chamber. Second, obtaining a sample by drilling can under-sample aggregate content which can result in inflated/overestimated conversion level. Although this issue is expected to be less concerning for carbonated concrete block than conventional concrete on account of its smaller particle sizes of aggregates, it is dealt with by calculating the hydrated lime content from TGA and comparing it with the expected proportion in the concrete mixture.

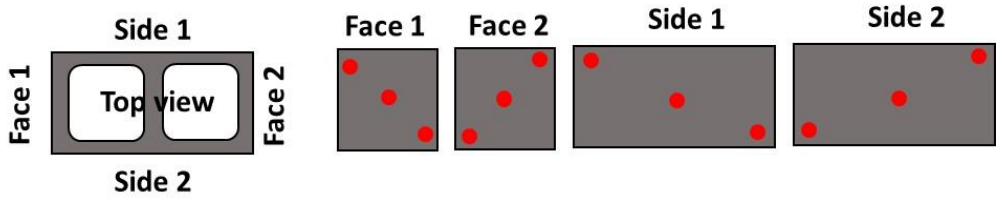

Figure 24: The powder sampling procedure for assessing CO_2 uptake of carbonated concrete blocks. This consists of examining six samples from side 1 and side 2 and six samples from face 1 and face 2. The powder samples are extracted using a drill press at different locations as depicted by red points. The extracted powders will then be homogenized to create a representative sample of the entire concrete block.

At the end of the operation cycle, the CO_2 uptake of the carbonated blocks was assessed/verified using thermogravimetric analysis (TGA: STA 6000, Perkin Elmer). Around 40 mg of each powder was placed in pure aluminum oxide crucibles and heated at a rate of 15 °C/min over a temperature range of 35 °C to 975 °C under UHP-N_2 gas purge at a flow rate of 20 mL/min. The CO_2 uptake is quantified by assessing the mass loss associated with $CaCO_3$ decomposition over the temperature range of 550 °C to 950 °C,[13] normalized by the total mass of solids in the binder (i.e., portlandite, fly ash, and cement). To this end, the mass loss associated with $CaCO_3$ is initially normalized by the total mass of initial dry solids (i.e., aggregate + binder solids and excluding the evaporable water content which is lost during heating to 120 °C) in the form of g_{CO2}/g_{solid}. The results are then normalized by the fraction of binder present in the total solids (i.e., $g_{CO2}/g_{solid} * g_{solid}/g_{reactants} = g_{CO2}/g_{reactants}$), which is determined from the mixture proportions. It should be noted that the CO_2 contents of fully cured blocks are subtracted from initial CO_2 content of pre-cured blocks upon its delivery to the host site.

The acceptance criterion of concrete masonry units defined in ASTM C90[15] dictates a net area compressive strength of 13.8 MPa (average of 3 units) and 12.4 MPa (individual units) at the time of delivery to the purchaser. For the sake of the demonstrations, it was assumed that the time of delivery is equivalent to 28 days from the initial batch preparation (starting with production at TCC). The units

selected as compression specimens are stored continuously in the air at a temperature of 24 °C ± 8 °C and relative humidity of less than 80 % for not less than 48 h. The net area compressive strength of the unit was calculated as follows:

$$Net\ area\ compressive\ strength\ (MPa) = P_{max}/A_n \quad \textbf{(Eq. 22)}$$

where P_{max} is the maximum compressive load (N) and A_n is the net area (mm^2) which is quantified as:

$$Average\ net\ area, A_n(mm^2) = (V_n \times 10^3)/H \quad \textbf{(Eq. 23)}$$

where H is the net height of the specimen (mm) and V_n is the net volume of the specimen (cm^3) which is calculated as follows:

$$Net\ volume, V_n(cm^3) = (w_s - w_i) \times 10^3 \quad \textbf{(Eq. 24)}$$

Table 15 summarizes the data to be recorded during block testing after completion of processing.

Table 15: A summary of characterization data that will be acquired and recorded during testing of fully cured blocks after the completion of processing.

#	Step	Data recorded during step	Method of measurement	Method of recording
5.A	Measurement of maximum compressive load of blocks	Maximum compressive load	Load cells	Hand-recording in data log
5.B	Net area measurement of selected blocks	Net area of each block	Displacement method of volume calculation and measurement	Hand-recording in data log
5.C	Thermal analysis of selected blocks	CO_2 content	Thermogravimetric analysis	Automatic recording of TGA traces in .txt file; recording of processed data using MATLAB and Excel spreadsheets

The difference in the average CO_2 content in the blocks over the course of processing was used to supplement and verify the mass balance on CO_2 calculated via on-line instrumentation. The maximum compressive load and the net area was used to calculate the compressive strength of the blocks in order to compare to the ASTM C90 performance criterion.

7.3.2 *System installation at host sites including insulation, chamber instrumentation, and internal gas flow distributors*

Figure 25 presents photographs of the system in various stages of installation. The primary installation steps were performed as follows for the ITC demonstration:

1. Install curing chamber and skid onto foundations
2. Install chamber-skid connecting piping and blower F-107 on top of curing chamber
3. Erect steel enclosure around system
4. Install exhaust stack
5. Connect system flue gas inlet to site flue gas header
6. Connect system water inlet to site water supply
7. Install wastewater tank
8. Install grounding rods
9. Install electrical panels and tie in to supply panel
10. Install building lighting and heaters (LV panel)
11. Connect system to site electrical (HV panel)
12. Install air-cooled water chiller and tie-in water line to system, power to HV panel
13. Install instrumentation tubing lines
14. Perform site walkdown with ITC staff to enable release of site power and flue gas
15. Install system insulation (spray foam and removable blankets)
16. Install system instrumentation
17. Install internal gas flow distributors

(a)

(b)

(c)

(d)

Figure 25: Photographs of **(a)** the completed steel enclosure on the ITC test bay, **(b)** the system exhaust stack and supporting guy wires, **(c)** the curing chamber with spray foam insulation applied, and **(d)** the site utility tie-ins.

The primary installation steps were performed as follows for the NCCC demonstration:

1. Install curing chamber and skid onto foundations
2. Install chamber-skid connecting piping and blower F-107 on top of curing chamber
3. Connect to site exhaust return
4. Connect system flue gas inlet to site flue gas header
5. Connect system water inlet to site water supply
6. Connect wastewater line to site return
7. Install grounding rods
8. Install electrical panels and tie in to supply panel
9. Connect system to site electrical (HV panel)
10. Install air-cooled water chiller and tie-in water line to system, power to HV panel
11. Install instrumentation tubing lines

12. Perform site walkdown with NCCC staff to enable release of site power and flue gas
13. Install piping insulation as per NCCC HAZOP
14. Install system instrumentation
15. Install internal gas flow distributors

7.3.3 *Operation*

7.3.3.1 System operations at Wyoming ITC host site

In total, 12 operational (production) runs were completed at the ITC host site. Each run comprised the following steps:

- Batch production (mixing and forming) at TCC Materials plant in Rapid City, SD
- Block semi-curing at TCC Materials to gain sufficient strength for transportation
- Unloading/palletizing
- Transportation of blocks to ITC host site
- Weighing of blocks and loading into carbonation curing chamber
- Processing (drying/carbonation/humidification/purge)
- Unloading of blocks, palletizing, weighing, sampling, and testing

Table 16 displays the summary of batch operation durations and major process performance data. Some notes on the operational batches follow:

- Batches A1-A5 were operated discontinuously (i.e., with time gaps between batches), while Batches B1-B7 were operated continuously (i.e., with batches run back-to-back).
- In Batch A1, the humidification process injected water constantly during the humidification step, which was observed to be inefficient because a large amount of water remained unabsorbed. In subsequent batches, the humidification step was changed such that the curing chamber was first cooled either by cycling without heating or purging the chamber with ambient air. Upon reaching the desired temperature, the water injection step was initiated and continued for a duration of 6 h.
- The initial batches (A1-A4) used an air-drying step before the carbonation step.
- Batch A5 was a trial for direct carbonation without using the drying step. Batches A5-B6, and Batch B7 used carbonation directly without a drying step. This alteration to the process significantly reduced energy input due to the shorter processing duration.
- Batch B6: The processing for this batch was modified further. The processing step consisted of adrying step followed by a carbonation step. However, during the carbonation step, the ITC control room turned off the flue gas supply to the test center. This process disruption was observed by the team approx. 3.5 h after the shutoff, upon which we radioed the control room to turn the flue gas back on. An additional 3.5-h duration was added to the carbonation step. This disruption caused a deviation in the CO_2 conversion trends from the typical values.
- Batch B7: The mixture proportions for Batch B7 were modified to incorporate a water-repellant admixture, which is typically utilized in concrete masonry products to control efflorescence. The processing conditions were similar to the standard procedure (i.e., direct carbonation without drying step).

Table 16: Summary of operational durations and main performance data per operational batch at the Wyoming ITC.

#	Operational productive hours, [system]	CO_2 uptake / input (kg) and [CO_2 utilization efficiency %]	Product mass (metric tons)	Total energy input (kWh)	Total water input (kg)	System water collected/ recovered (kg)
A1	113 [86.2]	284 / 382 = 74.4%	12.03	2719	1416	501
A2	113 [87.7]	191 / 327 = 58.3%	12.47	2769	733	473
A3	116 [87.5]	199 / 353 = 56.4%	12.37	2395	681	556
A4	126 [95.8]	226 / 347 = 65.2%	12.53	2348	725	526
A5	106 [78.4]	258 / 387 = 66.7%	12.53	1921	762	529
B1	104 [76.4]	272 / 444 = 61.3%	12.99	1792	758	486
B2	95 [65.4]	268 / 393 = 68.3%	13.09	1782	756	543
B3	98 [68.4]	289 / 352 = 82.1%	13.26	1749	799	418
B4	111 [81.1]	245 / 327 = 75.1%	13.15	1606	817	469
B5	128 [97.0]	248 / 306 = 80.9%	13.15	1835	869	494
B6	117 [88.0]	217 / 266 = 81.4%	13.27	1961	666	496
B7	118 [88.6]	228 / 315 = 72.3%	13.21	1819	659	449
Avg	**128 [83.4]**	**244 / 350, 70.2%**	**12.84**	**2058**	**803.5**	**495**
Sum	**1346 [1000]**	**2925/4200 = 69.7%**	**154.1**	**24693**	**9641.8**	**5939**

The CO_2 uptake (i.e., CO_2 removed from the gas stream and mineralized within the carbonated concrete blocks) over a 24-h carbonation duration was determined via the system's own instrumentation and thermogravimetric analysis, as described in the measurement and verification plan above. The CO_2 input into the system during this period was determined via system instrumentation. The CO_2 utilization efficiency % was determined as the average CO_2 uptake divided by the CO_2 input over the 24-h carbonation period. The CO_2 input into the system was calculated by calculating the mass flow rate of CO_2 into the system, from the measurements of CO_2 concentration and flow rate at the system inlet. The measured CO_2 concentration was corrected for the concentration of water vapor in the flue gas, which was determined based on the system inlet relative humidity/temperature sensor readings and flow rate

measurements. The gas flow rate calculations accounted for the dependence of flow rate on gas density and its composition. Similar calculations were performed for various locations in the system.

Figure 26 displays representative plots of the CO_2 concentration, temperature, and relative humidity, and flow rates of the gas streams at various locations in the system during the 24-h carbonation step during Batch B7. The CO_2 concentration at the system inlet was nearly constant, as it indicates the CO_2 concentration from the raw flue gas at the ITC. The CO_2 concentration of the system exhaust slowly rises from zero over the course of the carbonation step, as the CO_2 uptake of carbonated concrete blocks' reactants reduces in time.

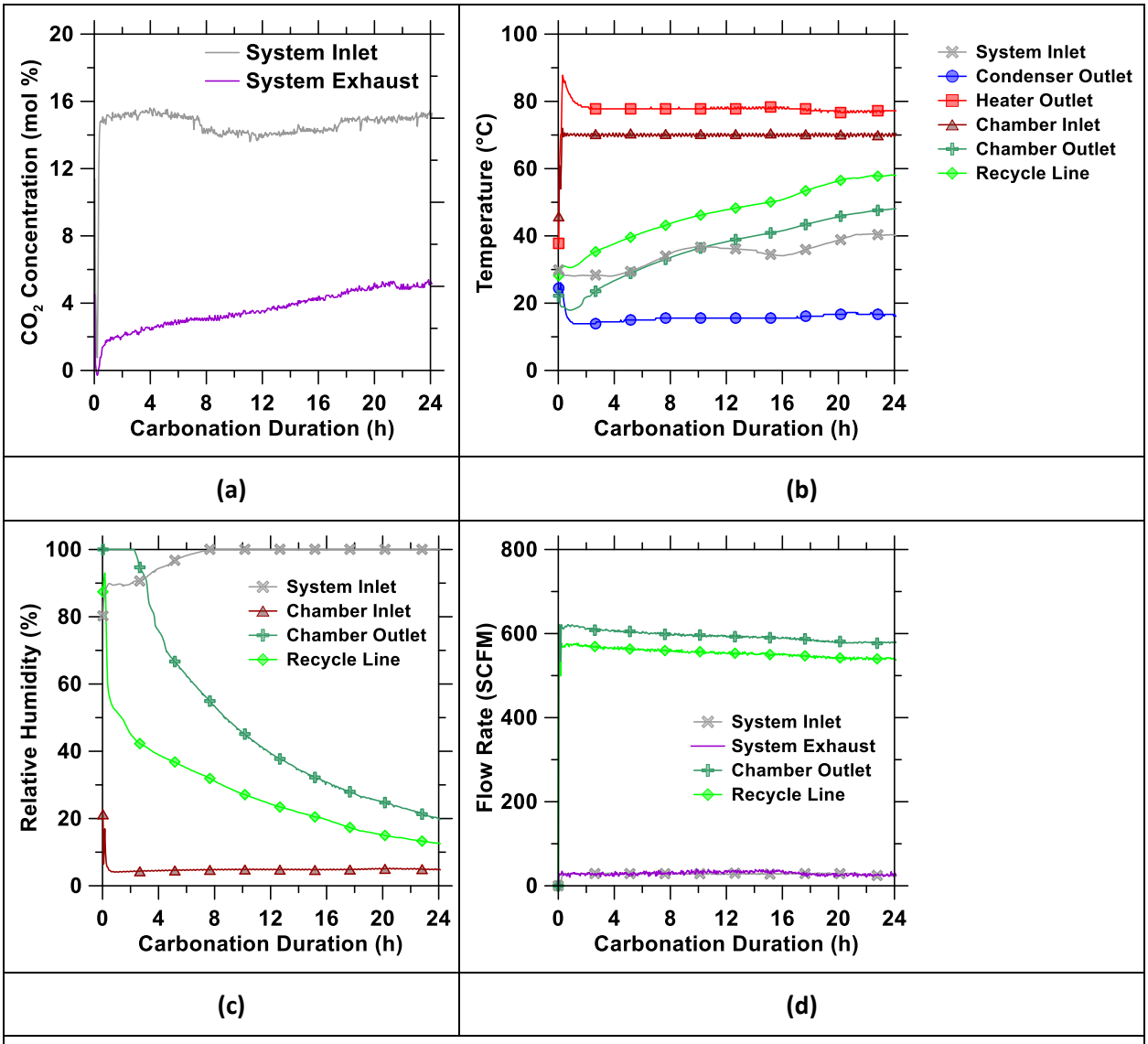

Figure 26: Representative plots of **(a)** CO_2 concentration, **(b)** temperature, **(c)** relative humidity, and **(d)** flow rates of the gas streams in various locations in the system during the 24-h carbonation step. This data was sourced from Batch B7.

The gas stream temperatures are indicated in Figure 26(b). The system inlet temperature generally increases as the system is heated and fluctuates in relation to ambient temperatures. This is because the flue gas travels a long distance from the ITC's blower through a distribution system to the test bay, over which the temperature of the gas may drop. After entering the system, the flue gas passes through the heat exchanger (condenser) to be cooled and drop out condensate water. The cooled gas then passes through two heaters to elevate the temperature for reaction. During carbonation, the system's heaters were controlled to the chamber's inlet temperature. The initial overshoot of the heater temperature and heat loss from the heater to the chamber inlet can be identified in Figure 26(b). As the heated gas flows through the chamber, heat is transferred to the curing chamber and blocks within it; the temperature of the gas stream exiting the curing chamber is progressively elevated as the temperature of the blocks rises. The recycle line temperature mimics the chamber outlet temperature but is higher because of the additional energy input into the gas stream by the induced draft blower between the chamber outlet and recycle line. The measured relative humidity values are shown in Figure 26(c).

Figure 26(d) shows the measured system flow rates. It can be seen that the system inlet and system exhaust flow rates are equivalent, as expected by the conservation of mass. The chamber outlet flow rate is significantly larger than these rates due to the high recycle ratio used. The recycle line flow rate is less than the chamber outlet by an amount equivalent to the exhaust flow rate, as expected.

Figure 27 displays the CO_2 conversion performance of a representative batch (Batch B7). The cumulative CO_2 input was computed from the system inlet flow rate and CO_2 concentration. The CO_2 uptake was determined in two ways: (1) from the difference in CO_2 mass flow rates between the system inlet and system exhaust, and (2) from the difference in chamber inlet and outlet mass CO_2 mass flow rates. The CO_2 utilization efficiency was calculated as the CO_2 uptake into the carbonated concrete blocks divided by the CO_2 input into the system. Each batch demonstrated CO_2 uptake trends similar to that of Figure 27, with some variations due to changes in system inlet flow rates, mixture compositions, and the specific processing conditions that were applied.

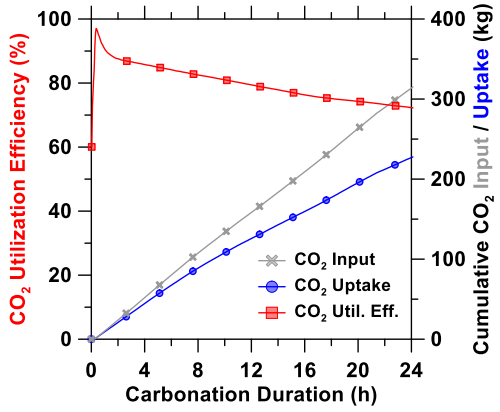

Figure 27: Representative plot of cumulative CO_2 input into the system, cumulative CO_2 uptake into the carbonated concrete blocks, and CO_2 utilization efficiency as a function of 24-h carbonation duration in Batch B7.

The cumulative CO_2 uptake into the carbonated concrete blocks and CO_2 utilization efficiency as a function of the 24-h carbonation period for all 12 demonstration runs are shown in Figure 28(a). System performance fulfilled the design specifications including (1) achieving in excess of 75% CO_2 utilization efficiency and (2) utilizing greater than 250 kg of CO_2 per run. The performance of the system was further analyzed in terms of energy and water usage.

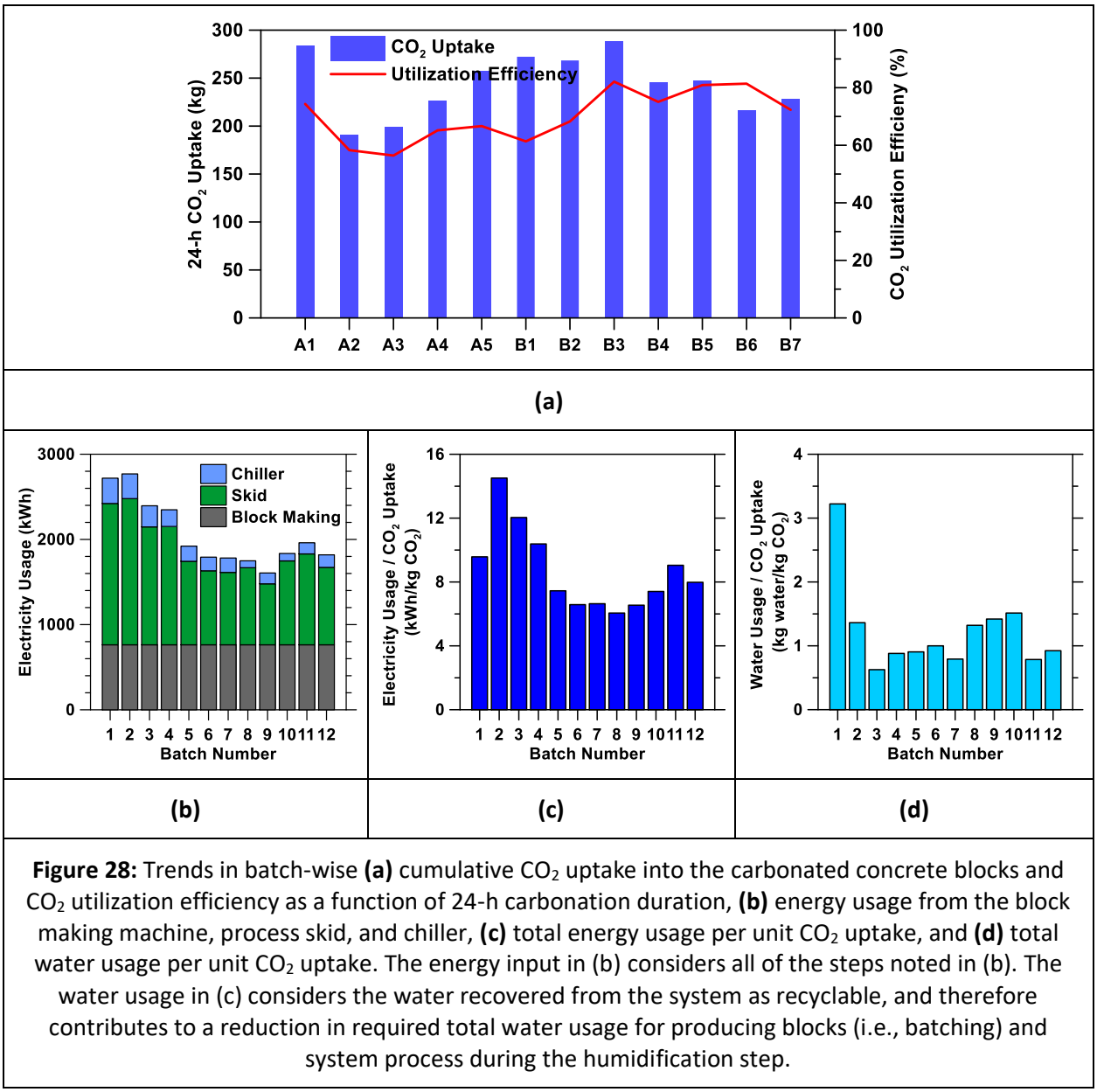

Figure 28: Trends in batch-wise **(a)** cumulative CO_2 uptake into the carbonated concrete blocks and CO_2 utilization efficiency as a function of 24-h carbonation duration, **(b)** energy usage from the block making machine, process skid, and chiller, **(c)** total energy usage per unit CO_2 uptake, and **(d)** total water usage per unit CO_2 uptake. The energy input in (b) considers all of the steps noted in (b). The water usage in (c) considers the water recovered from the system as recyclable, and therefore contributes to a reduction in required total water usage for producing blocks (i.e., batching) and system process during the humidification step.

Figure 28(b) shows the electricity usage of the process as a function of the batch number. The electricity usage can be attributed to block manufacturing (i.e., mixing, forming, and conveying), the system's process skid, and the system's chiller. The energy attributed to block manufacturing was estimated as a

constant based on the energy costs estimated by the producer. The energy usage of the process skid is primarily attributed to the electric heaters, with the blowers comprising the second largest skid energy usage. Significant reductions in energy usage were made over the course of operations, owing to the reduction in temperature setpoint and removal of the 24-h drying step prior to carbonation. These process improvements yielded an appreciable reduction in energy usage without sacrificing CO_2 uptake performance, as indicated by Figure 28(c). The water usage rate of the system was also improved over the course of operations, as the design of the humidification step was altered to increase its efficiency (Figure 28d). The water usage considers the recycling of water condensate recovered in the systems wastewater reservoir that was collected over the course of operation.

The performance of the CMUs produced during system operations was assessed against the relevant industry standard for conventional concrete masonry units (ASTM C90) at the TCC Materials site as well as a certified testing lab (BASF Corp. Construction Chemicals Division). The net area compressive strength of the CMUs was measured as per ASTM C140 at 28 days of age. The compressive strength was measured for each batch (see Figure 29), with the average compressive strength determined as 17.9 ± 1.22 MPa. The compressive strength of the blocks fulfilled the compressive strength specified by ASTM C90 (i.e., 13.8 MPa).

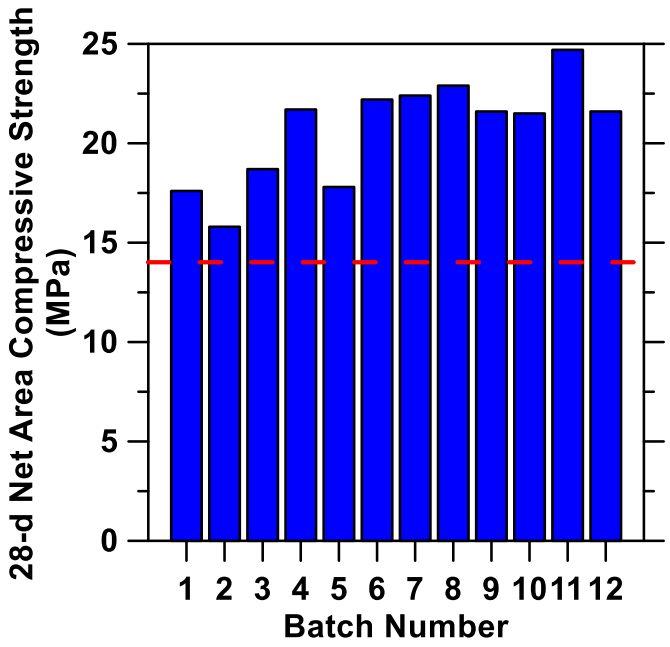

Figure 29: The average 28-day net area compressive strengths of carbonated concrete masonry units.

The oven-dry density and water absorption are the remaining performance characteristics for concrete masonry units. Water absorption and density measurements were carried out following the procedure of ASTM C140. The oven-dry density values of the carbonated concrete blocks range from 1900-to-2085 kg/m^3, which are considered “medium weight” and “normal weight” blocks as defined by ASTM C90. The

water absorption values range from 136-to-168 kg/m^3, which is below the ASTM C90 limits of 240 kg/m^3 and 208 kg/m^3 for medium weight and normal weight blocks, respectively.

7.3.3.2 System operations at Alabama NCCC host site

In total, 6 operational (production) runs were completed at the Alabama NCCC host site. Each run comprised the following steps:

- Batch production (mixing and forming) at Blair Block plant in Childersburg, AL
- Block semi-curing at Blair Block to gain sufficient strength for transportation
- Unloading/palletizing
- Transportation of blocks to NCCC host site
- Weighing of blocks and loading into carbonation curing chamber
- Processing (carbonation/purge)
- Unloading of blocks, palletizing, weighing, sampling, and testing

Table 17 displays the summary of batch operation durations and major process performance data.

Table 17: Summary of operational durations and main performance data per operational batch at the Alabama NCCC. The average values from the ITC demonstration have been included as a comparative test run.

#	Total curing cycle, [carbonation]	CO_2 uptake / input (kg) and [CO_2 utilization efficiency %]	Finished product mass (metric tons)	Process electricity usage (kWh)
ITC-average	118 [24]	257 / 343 = 74.9%	13.20	782
N1	26.25 [18.25]	96.8/312.1 = 31.0%	12.83	300.0
N2	26 [18]	140.97/192.6 = 73.2%	12.61	317.4
N3	26 [18]	178.2/233.6 = 76.3%	12.32	374.0
N4	26.1 [18.1]	91.3/204.5 = 44.6%	12.64	373.0
N5	26.1 [18.1]	118.6/177.5 = 66.8%	12.24	457.0
N6	26.1[18.1]	145.9/205.0 = 71.1%	13.01	390.0
Avg (N1-N6)	26.1 [18.1]	127.9/220.9 = 57.9%	12.69	368.57
Sum (N1-N6)	156.5 [108.5]	767.30	75.65	2211.40

Some notes on the operational production batches are as follows:

- Batches N1-N6 were operated continuously (i.e., with batches run back-to-back).
- Following learnings from the ITC demonstration, batches N1-N6 only applied a carbonation step without the drying and humidification steps. This alteration to the process significantly reduced energy input due to the shorter processing duration (reduced to 18-h). Each batch was exposed to the same carbonation curing time. The entire curing regime (precuring + carbonation curing) was limited to 26 h to match commercial block production cycle times.
- Batches were varied in terms of the input gas processing conditions, flue-gas supply source and formulation alteration.
- A two-step gas processing method was implemented to improve energy usage. Each production run utilized an initial high temperature period followed by a low temperature period. Each batch used the chiller to remove water.
- Batches N1-3 and N6 were cured using coal flue gas with an average CO_2 concentration of 12.2% and temperature of 112.5 °F leaving the gas scrubbers. The temperature dropped by 5-15 °F between gas scrubbers and the gas processing skid due to the large length of the piping.
- Batches N4 and 5 were cured using natural gas (NG) flue gas with an average CO_2 concentration of 3.9% and temperature of 71.6 °F. The NG boiler produced an outlet concentration of 8-9% and 110 °F, therefore the gas stream was diluted with air to produce a flue gas more representative of a commercial NG boiler (4-5%). This caused the temperature to decrease below the expected, 250-300 °F range.
- Higher portlandite content of the concrete was used for batches N1-5 except for N6 where half as much portlandite was used. This served to assess whether the same CO_2 conversion of the flue gas could be achieved using a lower portlandite content.
- Produced ~89 tonnes of block in 6 runs with 0.77 tonnes of CO_2 uptake.

The baseline performance targets of the carbonated concrete mineralization system and carbonated concrete blocks at the NCCC demonstration are summarized as follows:

- Fulfill the entire "curing regime" (precuring plus carbonation curing), in ~24 h to match commercial block production cycle times,
- CO_2 utilization efficiency > 70 %. This target could vary, however, as a function of CO_2 concentration of the flue gas stream
- At least 25 % lower process energy demand as compared to the ITC demonstration via process optimization
- Reduce process electricity usage per unit of CO_2 uptake as compared to ITC demo

The total curing time of 8-h steam curing at Blair Block followed by the 18-hour carbonation step exceeded the target curing time of 24-h by 2 h. However, 26-h curing time is still comparable to the industry standard for CMU production.

The CO_2 uptake (i.e., CO_2 removed from the gas stream and mineralized within the carbonated concrete blocks) was calculated by the same method reported in Section 7.3.3.1.

Figures 30a) and b) display the CO_2 conversion performance of a representative batch using coal and NG flue gas, respectively (Batch N3 and N5, respectively). The cumulative CO_2 input was computed from the system inlet flow rate and CO_2 concentration. The CO_2 uptake was determined in two ways: (1) from the difference in CO_2 mass flow rates between the system inlet and system exhaust, and (2) from the difference in chamber inlet and outlet mass CO_2 mass flow rates. The CO_2 utilization efficiency was

calculated as the CO_2 uptake into the carbonated concrete blocks divided by the CO_2 input into the system. Each batch demonstrated CO_2 uptake trends similar to that of Figure 30, with some variations due to changes in system inlet flow rates, mixture compositions, and the specific processing conditions that were applied.

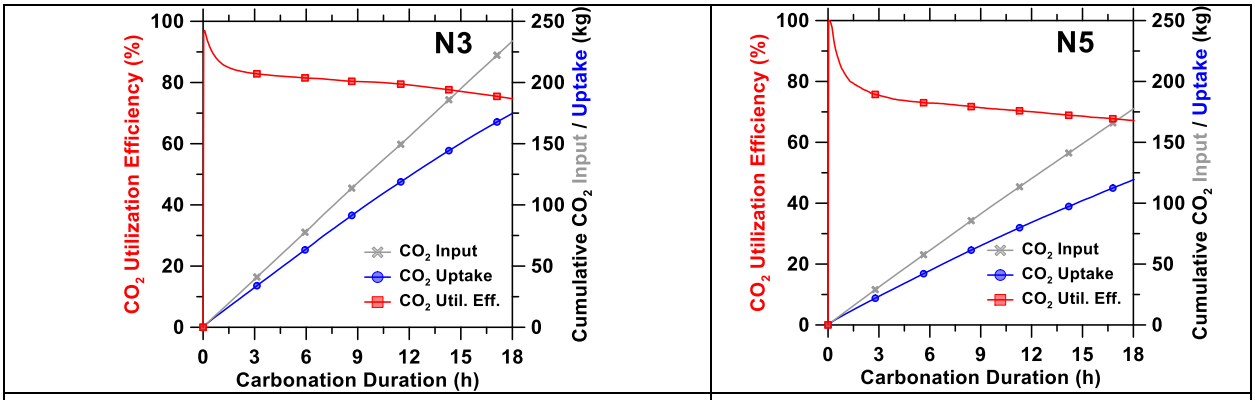

Figure 30: Representative plot of cumulative CO_2 input into the system, cumulative CO_2 uptake into the carbonated concrete blocks, and CO_2 utilization efficiency as a function of 18-h carbonation duration in Batch a) N3 – coal flue gas, and b) N5 natural gas flue.

The cumulative CO_2 uptake into the carbonated concrete blocks and CO_2 utilization efficiency as a function of the 18-h carbonation period for all 6 demonstration runs are shown in Figure 31(a). Three of the coal-fired production runs exceeded the target CO_2 utilization efficiency of 70%. Both NG flue gas batches were below this target value. However, the second, optimized batch (N5) achieved ~67% conversion. Further optimization to improve the CO_2 space velocity in the curing chamber will improve the conversion above the target value.

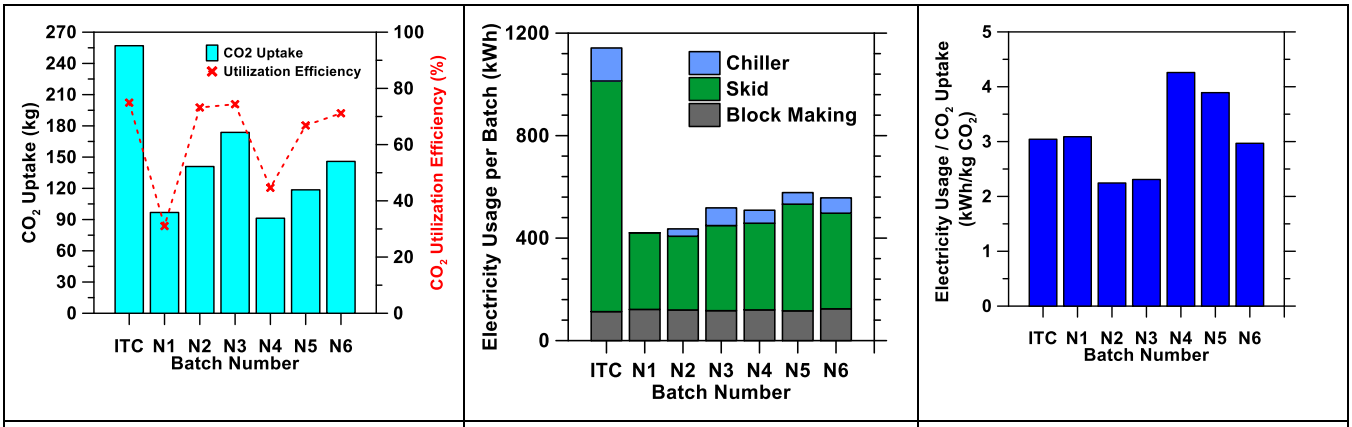

Figure 31: Trends in batch-wise **(a)** cumulative CO_2 uptake into the carbonated concrete blocks and CO_2 utilization efficiency as a function of 18-h carbonation duration, **(b)** energy usage from the block making machine, process skid, and chiller, **(c)** total energy usage per unit CO_2 uptake. The energy input in (c) considers all of the steps noted in (b).

Figure 31(b) shows the electricity usage of the process as a function of the batch number. The electricity usage was calculated using the same methodology as the ITC demonstration. Batch N1 featured the lowest energy usage as minimal gas processing was performed. The chiller was not used during this run, therefore no water was removed from the flue gas prior to entering the curing chamber. The higher humidity in the curing chamber reduced the effectiveness of gas transfer within the concrete blocks, thus limiting carbonation. For subsequent batches, the chiller was utilized which resulted in significant water removal and enhanced carbonation. Improved gas processing for the subsequent coal flue gas batches produced greater CO_2 uptake and energy efficiency, as shown in Figure 31(c). The revised two-step gas processing method and shorter curing time greatly reduced the total electricity usage for the NCCC batches when compared to the ITC average. For Batch N2, the electricity usage per unit of CO_2 uptake was 27.3% less than the average of the ITC demonstration. Reduction of total energy used and electricity usage per unit of CO_2 uptake achieved the final two targets for the NCCC demonstration. Energy reductions were lower for the NG batches as the low CO_2 concentration and inlet temperature required greater energy to improve the CO_2 uptake kinetics. More energy was required to maintain the curing chamber inlet temperature as the flue gas inlet temperature was 40.9 °F lower than that of the coal flue gas. Despite these limitations, the NG-flue gas still achieved CO_2 utilization efficiency of up to ~67%. The carbonated concrete technology would be expected to observe higher energy efficiency and uptake potential for commercial scale NG-boilers which operate at higher CO_2 concentrations and temperatures.

The compressive strength was measured for each batch, with the average compressive strength of the coal and NG flue gas determined to be 20.12 ± 1.31 and 20.87 ± 0.86 MPa, respectively (Figure 32). This compressive strength of the carbonated concrete blocks fulfilled the compressive strength specified by ASTM C90 (i.e., 13.8 MPa).

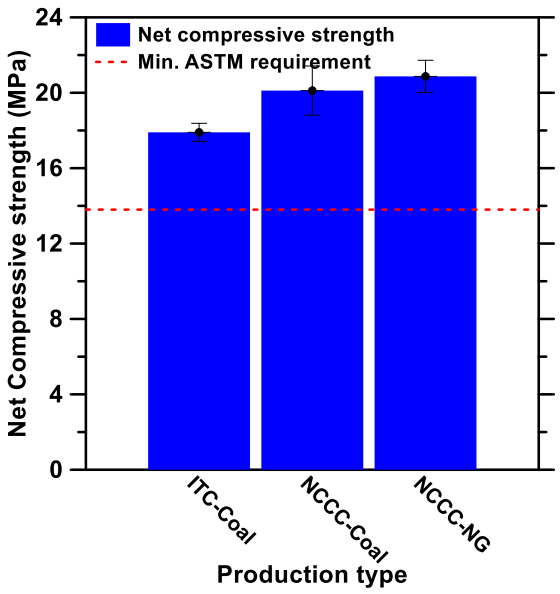

Figure 32: Net area compressive strength of the coal and NG flue gas concrete blocks.

As the Reversa process utilizes the CO_2 emissions from coal combustion, there may be a possibility of heavy metal and sulfur uptake during the carbonation process. This may lead to the formation of

secondary products from the contact of flue gas with the concrete. Based on X-ray fluorescence (XRF) analysis of the pre-carbonated and carbonated concrete blocks, no uptake of heavy metals was determined for both the coal and NG flue gas units. XRF performed on the blocks determined that all the heavy metals of interest from a TCLP test (arsenic, barium, cadmium, chromium, lead, mercury, selenium and silver) were undetectable. The low heavy metal content was also confirmed via acid-dissolution followed by ICP analysis. Figures 33a) and b) show that heavy metal content was < 0.01 wt.% of the carbonated and non-carbonated units for coal and NG exposure. This is a promising sign for the technology as this data does not show any uptake of harmful heavy metal contaminants. Accompanying the elemental analysis, a TCLP analysis was conducted via the NCCC staff to assess the leachability of the carbonated concrete blocks. All heavy metals were undetected in the analysis except for the presence of Ba (2.3 mg/L) in the coal flue gas units, which was far below the TCLP standard requirement of 100 mg/L.

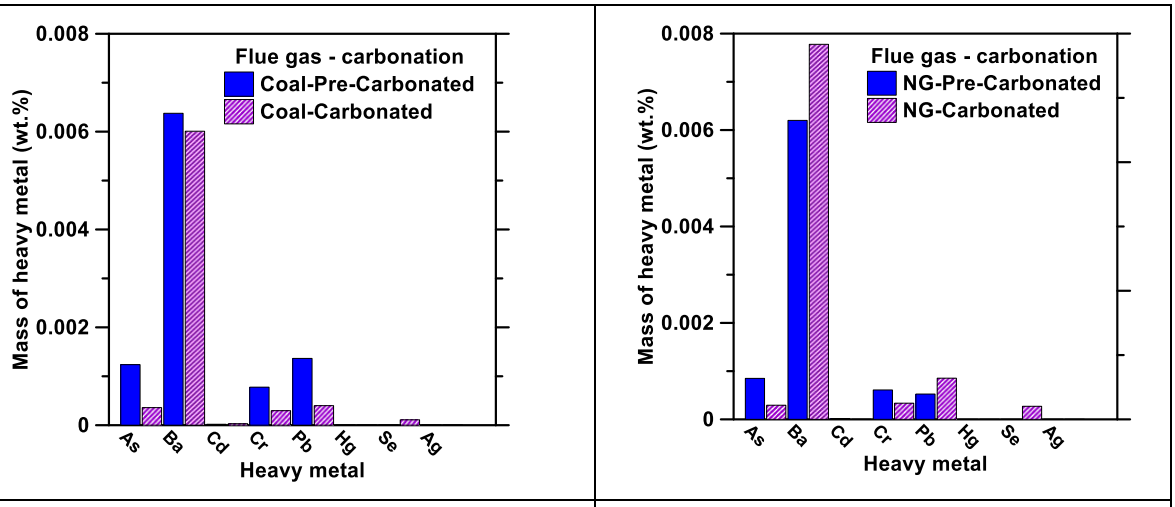

(a) **(b)**

Figure 33: The calculated weight percentage of heavy metals as determined by acid-dissolution followed by ICP analysis of the carbonated and non-carbonated concrete blocks considering **(a)** coal flue gas exposure and **(b)** NG flue gas exposure.

XRF analysis determined sulfur content of the concrete blocks to be approximately 0.35 wt.% for carbonated and non-carbonated concrete blocks as shown in Figure 34. Variation in sulfur content is minimal and differences shown are within standard deviation of each result. This indicates that sulfur uptake was negligible during the carbonation process. Furthermore, low sulfur uptake was expected as coal flue gas inlet contained < 1.05 ppm of SO_3. NG flue gas is expected to have a lower SO_3 content however, no instrumentation was available to account for SO_3 content in the NG flue gas stream.

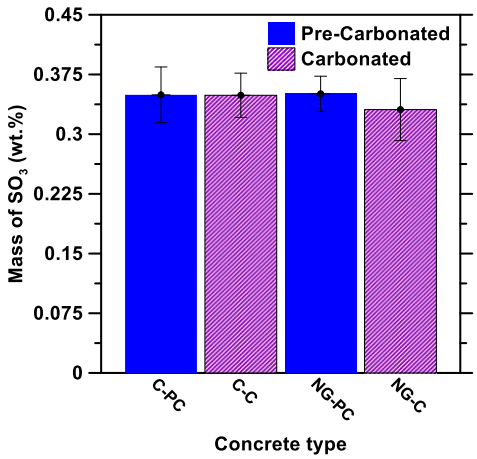

Figure 34: SO_3 content of CMU's pre-carbonated ('-PC') and carbonated ('-C') of coal ('C-') and NG ('NG-') flue gas blocks

7.3.4 *Project completion success criteria*

Based on the success criteria outlined in the Project Management Plan, the results of this project were a success. The quantification of the success metrics is displayed in Table 18.

Table 18: Success criteria for project DE-FE0031718 and whether these were achieved.

Success Criteria	**Achieved Value**
Carbonated concrete formulations demonstrate CO_2 uptake between 0.05 to 0.5 g CO_2/g reactant and compressive strength > 13.8 MPa for hollow-core block applications	• The ITC and NCCC demonstrations achieved an average of 0.19 and 0.1 g CO_2/g reactant, respectively. Both demonstrations exceeded the project's target goals. • Average compressive strength of the ITC blocks was 18.24 MPa at 28-days. This exceeded the target strength.
Field performance demonstrates 50 to 90% CO_2 utilization efficiency using real flue gas at host-site	ITC and NCCC produced an average CO_2 utilization efficiency of 74.9 and 57.9%, respectively. NCCC demo did reach highs of 75.6%. Both demonstrations were within the target range.
The Reversa process results in a construction material with a lifecycle footprint that is >25% smaller than OPC-concrete of equivalent performance grade.	An LCA of the Reversa process compared to an industry standard product revealed a net CO_2 reduction of 39% to 42%. This exceeds the target requirement.

7.4 Decommissioning

Figures 35 and 36 presents photographs of the system prepped and ready for transportation after the ITC and NCCC demonstrations, respectively. The key decommissioning steps were performed as follows for the ITC demonstration:

1. Uninstall curing chamber and skid onto foundations
2. Uninstall chamber-skid connecting piping on top of curing chamber
3. Disassemble steel enclosure around system. Send to UCLA for storage
4. Uninstall exhaust stack and dispose
5. Disconnect system flue gas inlet to site flue gas header
6. Disconnect system water inlet to site water supply
7. Uninstall wastewater tank and dispose
8. Uninstall grounding rods
9. Uninstall electrical panels and tie in to supply panel
10. Uninstall building lighting and heaters (LV panel). Pack for transport to NCCC
11. Disconnect system to site electrical (HV panel)
12. Uninstall air-cooled water chiller and tie-in water line to system, power to HV panel
13. Uninstall instrumentation tubing lines
14. Perform site walkdown with ITC staff to enable release of site power and flue gas
15. Uninstall system insulation (spray foam and removable blankets)
16. Uninstall system instrumentation
17. Uninstall internal gas flow distributors

(a)

(b)

Figure 35: Equipment loaded from ITC, ready for transport to NCCC: **(a)** gas processing skid, chiller, racks loaded onto a single truck and **(b)** curing chamber loaded onto a single truck.

The key decommissioning steps were performed as follows for the NCCC demonstration:

1. Disconnect curing chamber and skid onto foundations
2. Disconnect chamber-skid connecting piping on top of curing chamber
3. Disconnect to site exhaust return

4. Disconnect system flue gas inlet to site flue gas header
5. Disconnect system water inlet to site water supply
6. Disconnect wastewater line to site return
7. Uninstall grounding rods
8. Uninstall electrical panels and tie in to supply panel
9. Disconnect system to site electrical (HV panel)
10. Uninstall air-cooled water chiller and tie-in water line to system, power to HV panel
11. Uninstall instrumentation tubing lines
12. Uninstall system instrumentation
13. Uninstall internal gas flow distributors

Figure 36: Equipment loaded from NCCC, ready for future transport: overview of disconnected system at NCCC

8 Task 7.0 -Design and scalability analysis for commercial scale Reversa system

Details for this section were sent to DOE in a quarterly report during the course of the project. These details were not included in this report as they contain proprietary and confidential information.

9 Task 8.0 – Technoeconomic analysis and life cycle analysis

9.1 Technoeconomic analysis

Details for this section were sent to DOE in a quarterly report during the course of the project. These details were not included in this report as they contain proprietary and confidential information.

9.2 Life cycle analysis

The specific goal of this LCA is to compare the life cycle greenhouse gas impacts of the proposed product system (*blocks*) and the comparison product system (cement-based concrete block of an equivalent performance). The life cycle activities and related processes included in this cradle-to-gate LCA are the raw material supply, transportation, and manufacturing process. A simplified system boundary with reference flows is shown in Figure 37.

In modeling the LCA of the proposed and comparison product system, the following unit processes were considered: (1) aggregate production (natural) which corresponds to fine aggregates; (2) aggregate production (manufactured) which corresponds to coarse aggregates; (3) block plant operations (block forming and steam curing); (4) raw material transportation; (5) cement production; (6) portlandite production (for the proposed product system); and (7) Reversa carbonation processing. The cement LCI was taken from NREL USLCI.[37] The electricity source was considered as “US Fleet average coal electricity” provided in the openLCA NETL database. The electricity emission factors at the CMU production location are listed in Table 19. Table 19 also includes the assumptions and input data used in calculating the emissions from material transportation, raw materials production, and block plant operations.

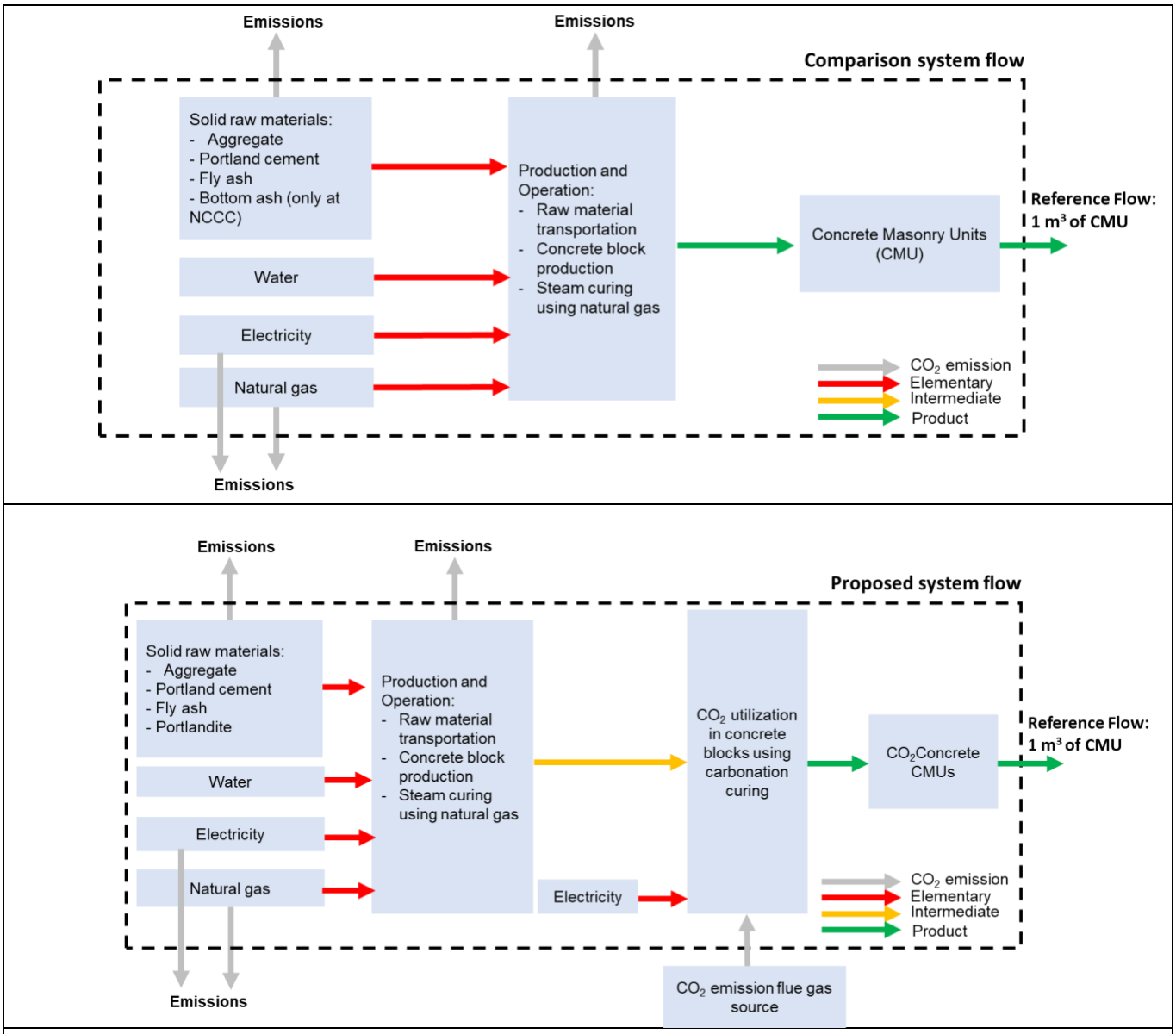

Figure 37: Simplified system boundaries for the comparison (top chart) and proposed (bottom chart) product systems considered in this LCA report.

Table 19: Input parameters used in the LCA model.			
Parameter description	**Input**	**Unit**	**reference/comment**
Material transportation			
Distance	20	miles	assumed
Average class 8 truck fuel consumption	5.29	mpg	U.S. Department of Energy [38]
diesel consumption for 20 miles	3.78	gallon	Calculated
Emission factor	10.18	kg CO_2/gallon diesel	EPA [39]
Total transportation emissions	38.49	kg CO_2	Calculated
Electricity			
Electricity emission factor for WY	0.94	kg CO_2/kWh	EPA [40]
Electricity emission factor for SD	0.24	kg CO_2/kWh	EPA [40]
Electricity emission factor for AL	0.394	kg CO_2/kWh	EPA [40]
Type of power plant	US Fleet average coal electricity		OpenLCA NETL database
Plant Operations			
Block forming electricity	8.56	kWh/tonne	Industry-average data from U.S. market
Curing steam	0.0106	MCF/tonne/h	Industry-average data from U.S. market
NCCC carbonation electricity	20.78	kW	Industry-average data from U.S. market
ITC carbonation electricity	36	kW	Industry-average data from U.S. market
Future scenario carbonation electricity	12	kW	Industry-average data from U.S. market
NG Emissions Factor	2	kg CO_2e/MCF	Industry-average data from U.S. market
Solar Emissions Factor	0.05	kg CO_2e/kWh	Industry-average data from U.S. market
CMU density	2100	kg/m^3	Industry-average data from U.S. market
Raw materials emission factors			
Ordinary Portland cement	0.928	kgCO_2/kg	OpenLCA-NREL database
Portlandite	0.768	kgCO_2/kg	OpenLCA-NREL database
Fly ash	0	kgCO_2/kg	Assumed
Coarse aggregate	0.00142	kgCO_2/kg	Marceau et al. [41]
Fine aggregate	0.00091	kgCO_2/kg	Marceau et al. [41]

The traditional CMU mixture formulation of ITC and NCCC projects were obtained from TCC Materials and Blair Block, respectively. The carbonated concrete block formulations were developed based on experimental research and adjusted based on some trial batches at the block manufacturing plant.

Third-party data: Third-party data used in the model are sourced from NETL, NREL, US EPA, and NRMCA, and industry average EPDs. The data used meets the technical, geographical, and temporal representativeness requirements defined in the Study Scope.

9.2.1 *Life Cycle Impact Assessment*

The purpose of this section is to document the impact assessment methods defined in the *Study Scope* to be included in the analysis. In this analysis, the NETL minimum requirement of life cycle GHG analysis using the IPCC AR5, 100-year time horizon characterization factors are implemented.

9.2.1.1 Life Cycle Impact Assessment Methods

The 100-year GWP factors for CO_2, CH_4, and N_2O utilized in this analysis are depicted in Table 20.

Table 20: IPCC AR5 GWPs .

GHG	20-year	100-year	Units
CO_2	1	1	kg CO_2e
CH_4	87	36	kg CO_2e
N_2O	268	298	kg CO_2e
SF_6	17,500	23,500	kg CO_2e

This analysis utilizes the latest factors available in TRACI 2.1, with modified *characterization factors* for GWP to reflect the current state of science from the IPCC.

9.2.1.2 Data Quality Assessment

The LCA data for the Comparison Product System does not include admixtures. The data sourced from the Portland Cement Association (PCA) omits admixtures because “the dosage rate of admixtures in concrete is typically well below one percent by mass”, consistent with the Society of Environmental Toxicology and Chemistry (SETAC) guidelines for conducting an LCA which “indicate that inputs to a process do not need to be included in an LCA is (1) they are less than 1% of the total mass of the processed materials or product…”. Additionally, fly ash and bottom ash are considered to have no associated inputs and outputs.

9.2.2 *Life Cycle Interpretation*

The life cycle impact assessment results for the proposed and comparison product systems are shown in Figure 38. The emissions from the carbonated concrete CMU for the ITC project site were calculated using two scenarios: (1) CMU block produced at the TCC Materials plant in South Dakota and carbon-cured at the ITC in Wyoming (electricity emission factors of SD and WY are used); (2) CMU block produced and carbon-cured at the TCC Materials plant in South Dakota (electricity emission of SD is used). The net

emissions from the production of one cubic meter of traditional CMU range from 324 to 356 kg CO_2e. Using the Reversa technology, the net emissions were lowered by 127 kg and 150 CO_2e which is 39% to 42% of the comparison product system for the NCCC and ITC sites, respectively.

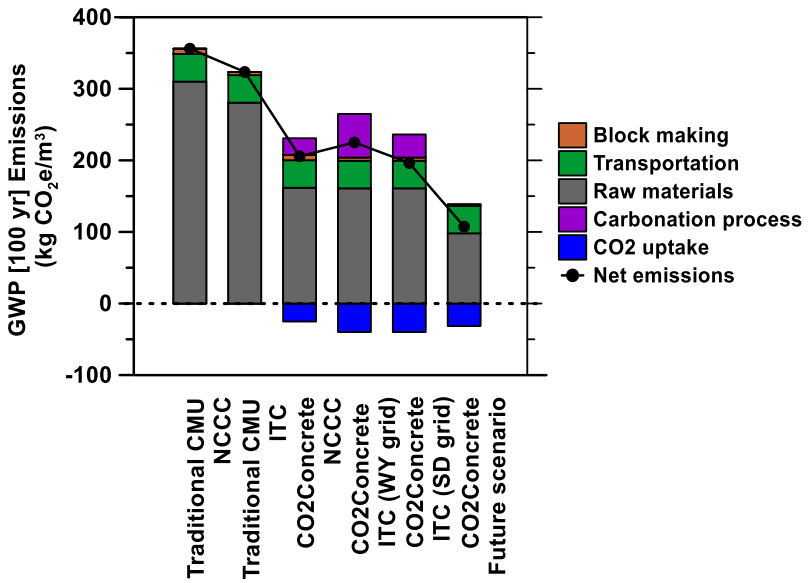

Figure 38: Comparison of cradle-to-gate emissions of 1 m^3 of traditional and carbonated concrete blocks at ITC and NCCC project sites. A future scenario targeted emission level is also presented.

10 References

[1] R. Andrew, Global CO_2 emissions from cement production, Earth System Science Data Discussions. 10 (2018) 195–217. https://doi.org/10.5281/ZENODO.831455.

[2] H.F.W. Taylor, Cement Chemistry, Thomas Telford, 1997.

[3] IEA, Energy Technology Perspectives 2016: Towards Sustainable Urban Energy Systems, 2016.

[4] P.K. Mehta, P.J. Monteiro, Concrete: Microstructure, Properties, and Materials, 3rd ed., McGraw-Hill Education, 2014.

[5] E.M. Gartner, D.E. Macphee, A physico-chemical basis for novel cementitious binders, Cement and Concrete Research. 41 (2011) 736–749. https://doi.org/10.1016/j.cemconres.2011.03.006.

[6] S.A. Miller, A. Horvath, P.J.M. Monteiro, Readily implementable techniques can cut annual CO 2 emissions from the production of concrete by over 20%, Environ. Res. Lett. 11 (2016) 074029. https://doi.org/10.1088/1748-9326/11/7/074029.

[7] IEA, CO_2 emissions from fuel combustion: Overview 2020, 2020.

[8] Z. Wei, B. Wang, G. Falzone, E.C. La Plante, M.U. Okoronkwo, Z. She, T. Oey, M. Balonis, N. Neithalath, L. Pilon, Clinkering-free cementation by fly ash carbonation, Journal of CO2 Utilization. 23 (2018) 117–127.

[9] National Academies of Sciences, Engineering, and Medicine, Gaseous Carbon Waste Streams Utilization: Status and Research Needs, The National Academies Press. https://doi.org/10.17226/25232, Washington, DC, 2018.

[10] I. Mehdipour, G. Falzone, E.C. La Plante, D. Simonetti, N. Neithalath, G. Sant, How Microstructure and Pore Moisture Affect Strength Gain in Portlandite-Enriched Composites That Mineralize CO2, ACS Sustainable Chemistry & Engineering. 7 (2019) 13053–13061.

[11] C. Jenewein, C. Ruiz-Agudo, S. Wasman, L. Gower, H. Cölfen, Development of a novel CaCO 3 PILP based cementation method for quartz sand, CrystEngComm. 21 (2019) 2273–2280.

[12] S.-Y. Pan, B. Lai, Y. Ren, Mechanistic insight into mineral carbonation and utilization in cement-based materials at solid–liquid interfaces, RSC Advances. 9 (2019) 31052–31061.

[13] K. Vance, G. Falzone, I. Pignatelli, M. Bauchy, M. Balonis, G. Sant, Direct carbonation of Ca (OH) 2 using liquid and supercritical CO2: implications for carbon-neutral cementation, Industrial & Engineering Chemistry Research. 54 (2015) 8908–8918.

[14] I. Mehdipour, G. Falzone, D. Prentice, N. Neithalath, D. Simonetti, G. Sant, The role of gas flow distributions on CO_2 mineralization within monolithic cemented composites: coupled CFD-factorial design approach, React. Chem. Eng. 6 (2021) 494–504. https://doi.org/10.1039/D0RE00433B.

[15] ASTM C90 − 16a: Standard Specification for Loadbearing Concrete Masonry Units, ASTM International, West Conshohocken, PA, 2016.

[16] ASTM Standard D4326-13: Standard Test Method for Major and Minor Elements in Coal and Coke Ash By X-Ray Fluorescence, ASTM International, West Conshohocken, PA, 2013. https://doi.org/10.1520/D4326-13.

[17] ASTM C618 - 19: Standard Specification for Coal Fly Ash and Raw or Calcined Natural Pozzolan for Use in Concrete, ASTM International, West Conshohocken, PA, 2019.

[18] H.H. Steinour, Some effects of carbon dioxide on mortars and concrete-discussion, J. Am. Concr. Inst. 30 (1959) 905–907.

[19] G.T. Rochelle, Amine scrubbing for CO2 capture, Science. 325 (2009) 1652–1654.

[20] D.K. Lee, An apparent kinetic model for the carbonation of calcium oxide by carbon dioxide, Chemical Engineering Journal. 100 (2004) 71–77. https://doi.org/10.1016/j.cej.2003.12.003.

[21] C.F. Dickinson, G.R. Heal, Solid–liquid diffusion controlled rate equations, Thermochimica Acta. 340–341 (1999) 89–103. https://doi.org/10.1016/S0040-6031(99)00256-7.

[22] M. Castellote, L. Fernandez, C. Andrade, C. Alonso, Chemical changes and phase analysis of OPC pastes carbonated at different CO2 concentrations, Mater Struct. 42 (2008) 515–525. https://doi.org/10.1617/s11527-008-9399-1.

[23] D.T. Beruto, R. Botter, Liquid-like H2O adsorption layers to catalyze the Ca(OH)2/CO2 solid–gas reaction and to form a non-protective solid product layer at 20°C, Journal of the European Ceramic Society. 20 (2000) 497–503. https://doi.org/10.1016/S0955-2219(99)00185-5.

[24] S.-M. Shih, C.-S. Ho, Y.-S. Song, J.-P. Lin, Kinetics of the Reaction of Ca(OH)2 with CO2 at Low Temperature, Ind. Eng. Chem. Res. 38 (1999) 1316–1322. https://doi.org/10.1021/ie980508z.

[25] ASTM C150/C150M − 18: Standard Specification for Portland Cement, ASTM International, West Conshohocken, PA, 2018.

[26] ASTM C618 − 15: Standard Specification for Coal Fly Ash and Raw or Calcined Natural Pozzolan for Use in Concrete, ASTM International, West Conshohocken, PA, 2015.

[27] ASTM C33/C33M − 18: Standard Specification for Concrete Aggregates, ASTM International, West Conshohocken, PA, 2018.

[28] ASTM C305 − 14: Standard Practice for Mechanical Mixing of Hydraulic Cement Pastes and Mortars of Plastic Consistency, ASTM International, West Conshohocken, PA, 2014.

[29] ASTM C128 − 15: Standard Test Method for Relative Density (Specific Gravity) and Absorption of Fine Aggregate, ASTM International, West Conshohocken, PA, 2015.

[30] ASTM C39/C39M − 18: Standard Test Method for Compressive Strength of Cylindrical Concrete Specimens, ASTM International, West Conshohocken, PA, 2018.

[31] K. Vance, A. Kumar, G. Sant, N. Neithalath, The rheological properties of ternary binders containing Portland cement, limestone, and metakaolin or fly ash, Cement and Concrete Research. 52 (2013) 196–207.

[32] D. Wang, A. Bao, W. Kunc, W. Liss, Coal power plant flue gas waste heat and water recovery, Applied Energy. 91 (2012) 341–348.

[33] M. Shuangchen, C. Jin, J. Kunling, M. Lan, Z. Sijie, W. Kai, Environmental influence and countermeasures for high humidity flue gas discharging from power plants, Renewable and Sustainable Energy Reviews. 73 (2017) 225–235.

[34] X. Pang, D.P. Bentz, C. Meyer, G.P. Funkhouser, R. Darbe, A comparison study of Portland cement hydration kinetics as measured by chemical shrinkage and isothermal calorimetry, Cement and Concrete Composites. 39 (2013) 23–32. https://doi.org/10.1016/j.cemconcomp.2013.03.007.

[35] E.L. Cussler, Diffusion: mass transfer in fluid systems, Cambridge university press, 2009.

[36] F. Georget, J.H. Prévost, B. Huet, Impact of the microstructure model on coupled simulation of drying and accelerated carbonation, Cement and Concrete Research. 104 (2018) 1–12. https://doi.org/10.1016/j.cemconres.2017.11.008.

[37] National Renewable Energy Laboratory, U.S. Life Cycle Inventory Database | NREL, (2012). https://www.nrel.gov/lci/ (accessed October 14, 2019).

[38] Alternative Fuels Data Center, Average Fuel Economy by Major Vehicle Category, (n.d.). https://afdc.energy.gov/data/10310 (accessed April 12, 2021).

[39] EPA, Greenhouse Gas Emissions from a Typical Passenger Vehicle, (2014). https://nepis.epa.gov/Exe/ZyPDF.cgi?Dockey=P100U8YT.pdf.

[40] EPA, Emissions & Generation Resource Integrated Database (eGRID), (2018). https://www.epa.gov/egrid.

[41] M. Marceau, M. Nisbet, M. VanGeem, Life Cycle Inventory of Portland Cement Concrete, Portland Cement Association, 2006.

[42] IPCC, Climate Change 2013: The Physical Science Basis. Contribution of Working Group I to the Fifth Assessment Report of the Intergovernmental Panel on Climate Change, Cambridge University Press, Cambridge and New York, 2013.